Available online at www.sciencedirect.com
ScienceDirect
Journal of Fluorine Chemistry 128 (2007) 243–262
JOURNAL OF FLUORINE CHEMISTRY
www.elsevier.com/locate/fluor

Review

Fluoride based electrode materials for advanced energy storage devices

Glenn G. Amatucci *, Nathalie Pereira

Energy Storage Research Group, Department of Materials Science and Engineering, Rutgers, The State University of New Jersey, 671 US Highway 1, North Brunswick, NJ 08902, USA

Received 22 October 2002; accepted 27 November 2006
Available online 13 December 2006

Abstract

Energy storage and conversion have become a prime area of research to address both the societal concerns regarding the environment and pragmatic applications such as the powering of an ever increasing cadre of portable electronic devices. This paper reviews the use of fluoride based electrode materials in energy storage devices. The majority of the energy storage and conversion applications for fluorine based materials resides in present and future lithium battery chemistries. The use of fluorides either as coatings or in the formation of oxyfluorides has resulted in a marked increase of the stability and morphological development of electrodes for use in nonaqueous lithium and lithium-ion batteries. Pure fluorides, despite their intrinsic insulative properties, have demonstrated the capability to exhibit exceptional energy densities and have the potential to open the door to future high energy lithium battery technology.

Keywords: Fluorine; Fluorides; Energy storage; Batteries; Lithium; Electrode materials; Intercalation

Contents

* Corresponding author. Tel.: +1 732 932 6856; fax: +1 732 932 6855.
E-mail address: gamatucc@rci.rutgers.edu (G.G. Amatucci).

0022-1139/$ – see front matter © 2007 Published by Elsevier B.V.
doi:10.1016/j.jfluchem.2006.11.016

1. Introduction

Fluorine based materials have been gradually entering a prominent place in energy storage and conversion, resulting in materials of great performance and stability. While fluorides have been recently introduced in energy conversion applications such as electrolytes for fuel cells, transparent electrodes for solar cells, and electrodes for aqueous batteries, the application of fluorine based materials has manifested itself to a great extent in high energy lithium nonaqueous batteries. The use of fluorides stems from the intrinsic stability of fluorinated materials and their ability to generate high electrochemical energy as electrodes. Both of these attributes are a direct result of the extraordinary electronegativity of fluorine and exceptionally high free energy of formation of fluorides. The application of fluorine materials in lithium batteries spans from electrode materials to electrolytes. In the early years, the use of fluorine based electrolytes and binders established the stability of the electrochemical system at the extreme potentials at which they operate. Over the past two decades enormous quantity of work has been dedicated to the study of fluorinated salts for electrolytes [1–4], fluorinated binders to maintain structural integrity of the electrode composites, and most recently fluorinated solvents for increased stability and safety in Li-ion batteries. This rich subject matter will not be addressed herein due to space restrictions but readers are encouraged to investigate these developments [5]. Within this paper we turn to the application of fluorine derived materials as electrodes in batteries, although some materials have been in existence for a number of years, aspects of their operational mechanisms remain unclear. In addition, a number of new materials has recently been enabled by addressing the paradox of electrochemical activity through the use of nanoenabled complexes. This paper is focused on presenting a comprehensive review of these materials and also their sometimes controversial mechanisms which lead to their improved electrochemical activity.

2. Intercalation compounds

Novel routes have been investigated to improve the electrochemical performance of the intercalation materials previously developed for use as electrode materials for Li-ion batteries. These include layered transition metal oxides and lithium manganese spinels for the positive electrode, and carbonaceous materials for the negative. One alternative route consisted in the investigation of the fluorine chemistry through doping of the existing materials with fluorine. Two avenues were undertaken. The fluorine was either introduced into the bulk of the oxide-based materials by substitution of fluorine for oxygen throughout the entire lattice, or limited to the surface of materials via surface fluorination. Although fluorine doping was also applied to conversion materials such as tin oxide [6–8], we will limit ourselves to the review of intercalation materials doped with fluorine and its subsequent effect on materials electrochemical properties. We will also take a close look at novel fluoride-based intercalation materials such as fluorophosphates and $LiAMF_6$ compounds.

2.1. Fluorine-doped intercalation materials

2.1.1. Bulk doping

2.1.1.1. Layered transition metal oxyfluorides. Layered lithium transition metal oxides have been extensively studied for their electrochemical performance as high potential electrode materials for secondary Li-ion batteries. Although $LiCoO_2$ is the most famous, as it has been and still is widely used as material of choice in commercial cells. $LiNiO_2$ has also received tremendous attention due to its larger specific capacity over the same voltage range and lower cost. However, difficulties in synthesizing the stoichiometric compound were reported and lithium-deficient $Li_{1-x}Ni_{1+x}O_2$, where x depends on the synthesis conditions, showed poor cycling stability and poor thermal stability in the charged state. Both required improvements for practical use of $LiNiO_2$. Partial trivalent cation substitutions for nickel were first investigated to enhance cyclability. Although these cationic substitutions resulted in some improvement associated to improved cation ordering with decreased amounts of Ni^{2+} ions in the lithium layer obstructing lithium diffusion, and minimized structural deformations; lower rechargeable capacities were obtained. Kubo et al. [9] initiated the exploration of oxyfluorides as cathode materials with their work on $LiNiO_2$-based compounds. They investigated a series of $Li_{1+x}Ni_{1-x}O_{2-y}F_y$ compounds with $y < 2x$ fabricated by solid state synthesis at 650 °C in oxygen utilizing mixtures of $Li(OH)\cdot H_2O$, $Ni(OH)_2$ and LiF precursors. The excess lithium was utilized to maintain a nickel average oxidation number above 3 in order to minimize the nickel migration into the lithium layer. Although $Li_{1.08}Ni_{0.92}O_{1.9}F_{0.1}$ exhibited lower initial reversible capacity compared to $LiNiO_2$, reversible capacity increased within a couple of cycles and showed improved capacity retention during cycling (Fig. 1). The former was proposed to derive from the shifting of fluorine ions facilitating lithium movement in the crystal lattice during cycling. The latter was attributed to the presence of an extra phase transition in the monoclinic domain and to the absence at the end of charge of a transition to a short c-axis hexagonal phase, previously observed to be detrimental to cycle life. Although cycle life was improved in $Li_{1.08}Ni_{0.92}O_{1.9}F_{0.1}$ compared to $LiNiO_2$, a capacity fade close to 50% was still observed over 100 cycles between 3 and 4.3 V (Fig. 1). Based on previous studies showing cobalt substitution reduced

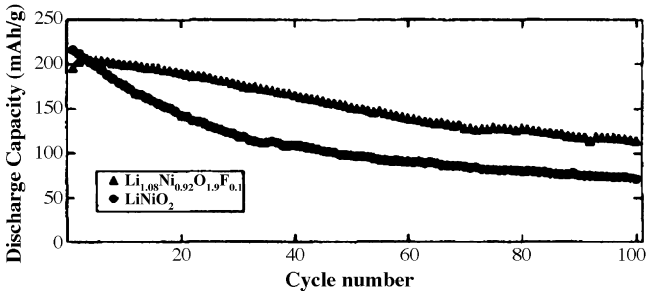

Fig. 1. Discharge capacity as a function of cycle number for $Li_{1.08}Ni_{0.92}O_{1.9}F_{0.1}$ compared to $LiNiO_2$ cycled vs. lithium metal between 3 and 4.3 V [9].

structural deformation [10,11], the authors proposed the co-substitution of cobalt and fluorine for nickel and oxygen, respectively with $Li_{1+x}Ni_{1-x-y}Co_yO_{2-z}F_z$ compounds [12] in an attempt to further enhance cycling performance. The $Li_{1+x}Ni_{1-x-y}Co_yO_{2-z}F_z$ compounds, with Co/Ni atomic ratios of 0.1 and 0.18 and $z = 0$–0.25, were fabricated by solid state synthesis at 675 °C in oxygen from mixtures of $Li(OH)\cdot H_2O$, LiF and co-precipitated $(Ni,Co)(OH)_2$. All compounds were identified as single phase by XRD analysis. The cobalt and fluorine co-substitution lead to a further decrease of the initial discharge capacity to 182 mAh/g for $Li_{1.075}Ni_{0.755}Co_{0.17}O_{1.9}F_{0.1}$, but dramatically improved cycle life with a 2.8% capacity decreases over 100 cycles between 3 and 4.3 V. The results also indicated that larger cobalt content required larger amounts of fluorine to suppress capacity fade. In order to clarify the role of fluorine in the electrochemical performance improvement of lithium nickelates, Naghash and Lee [13] investigated the sole effect of fluorine with the study of the electrochemical properties of lithium deficient $Li_{1-x}Ni_{1+x}O_{2-y}F_y$ compounds. These were obtained by dissolution of NiF_2 in a mixture of nitric and hydrochloric acid subsequently added to a mixture of $LiNO_3$ and $Ni(CH_3COO)_2\cdot 4H_2O$. The resulting precursors were submitted to various heat-treatments steps [14]. The positive impact of fluorine on coulombic efficiency and cycling stability (for materials with $y < 0.015$) was proposed to be associated to the reduction of nickel migration into the lithium layer induced by an increase of the Ni^{3+} ion migration activation energy resulting from the high-spin configuration of the Ni^{3+} cation surrounded by weak field ligand F^- anions.

As opposed to the positive effect on the structural properties of $LiNi_{1-y}M_yO_2$ observed with cobalt substitution, low amounts of manganese substitution in $LiNi_{1-y}Mn_yO_2$ compounds were reported to favor cation mixing and resulted in the deterioration of the electrochemical performance such as reversible capacity, polarization and cycling stability [15]. In spite of these results, the satisfying electrochemical properties obtained by Makimura and Ohzuku [16] for the peculiar $LiNi_{0.5}Mn_{0.5}O_2$ composition combined with the improvement of thermal stability observed with the addition of manganese promoted further investigation of the $LiNi_{0.5}Mn_{0.5}O_2$ system. $Li(Ni_{0.5+0.5z}Mn_{0.5-0.5z})O_{2-z}F_z$ $(0 \le z \le 0.2)$ samples were fabricated by solid state synthesis using a mixture of Li_2CO_3, LiF and (Ni_xMn_{1-x})-hydroxide [17]. The materials were heat-treated at 600 and 1000 °C in air. The analysis of the effect of fluorine substitution on the electrochemical behavior of $LiNi_{0.5}Mn_{0.5}O_2$ revealed improved initial internal cell impedance and cycling stability despite a larger degree of cation mixing. Although the improved impedance stability observed upon cycling was proposed to contribute to the enhanced capacity retention, the role of fluorine remained unclear.

$LiNi_{1/3}Co_{1/3}Mn_{1/3}O_2$, first reported by Ohzuku et al. [18,19] to deliver a high reversible capacity of 200 mAh/g over the 2.5–4.6 V voltage range with good rate capability and high thermal stability, spurred interest in the investigation of the Li–Ni–Co–Mn–O system. Sun and coworkers studied the effect of the addition of fluorine on the electrochemical properties of the

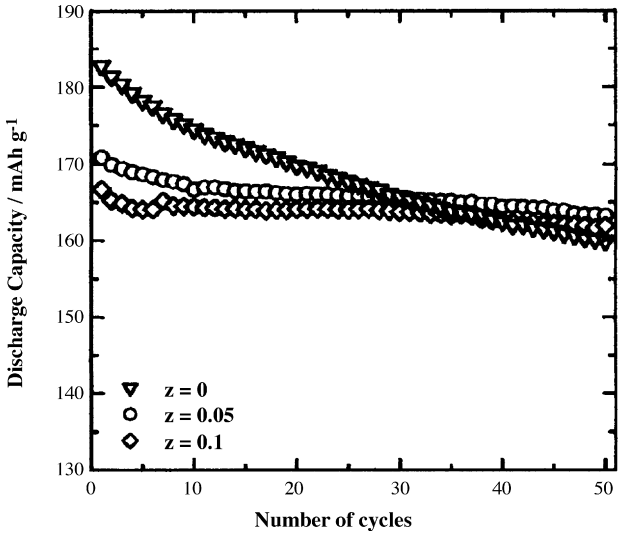

Fig. 2. Cycling performance of $Li(Ni_{1/3}Co_{1/3}Mn_{1/3})O_{2-z}F_z$ for $z = 0$, 0.05 and 0.1 cycled vs. lithium metal between 2.8 and 4.6 V at a 0.2C rate [20].

$LiNi_{1/3}Co_{1/3}Mn_{1/3}O_2$ [20,21], $LiNi_{1/3}Co_{1/3}Mn_{1/3-x}Mg_xO_2$ $(x = 0.04)$ [22] and $LiNi_{0.43}Co_{0.22}Mn_{0.35}O_2$ [23] compounds. The spherical non-fluorinated and fluorinated materials were fabricated from mixed hydroxides obtained by co-precipitation added to $LiOH\cdot H_2O$ and LiF (for the fluorinated compounds) and heat-treated at elevated temperature as described in more details in Ref. [24]. Unfortunately the $LiNi_{1/3}Co_{1/3}Mn_{1/3}O_2$ material obtained by this method exhibited poorer capacity retention than the materials fabricated by solid-state synthesis proposed by Yabuuchi and Ohzuku [19]. Although synthesis conditions have been shown to significantly affect the electrochemical performances of $LiNi_{1/3}Co_{1/3}Mn_{1/3}O_2$ [25], more work is required to clearly identify the root of the poorer cycling behavior of the undoped material obtained by co-precipitation. In this context, the investigation revealed the addition of small amounts of fluorine slightly decreased the material's initial discharge capacity but greatly improved capacity retention (Fig. 2), rate capability and thermal stability. The lower initial discharge capacity of the fluorine-doped materials was attributed to the stronger Li–F bonds that hinder lithium movement during charge. The strong Li–F bonds may also partially offset the electrostatic repulsion between the Ni–O slabs occurring during delithiation consistent with smaller *c*-axis elongation compared to that observed for $LiNi_{1/3}Co_{1/3}Mn_{1/3}O_2$ during charge. The physical properties of the materials were also affected by the addition of fluorine. The primary particles grew in size with increasing fluorine content, while the morphology of the particles changed from round to well-developed polygons (Fig. 3). Similar morphology changes had been previously observed with $LiMn_2O_4$ spinels [26]. These physical changes resulted in increased tap-density. High density is a desirable material characteristic to fabricate electrodes of high volumetric capacities. Indeed, the fluorine-doped materials exhibited larger volumetric capacities despite lower gravimetric capacities. These results agree well with the use of LiF as sintering agent for the preparation of denser $Li(Ni_xCo_{1-2x}Mn_x)O_2$ materials $(x = 0.1$ and $0.25)$ [27]. In

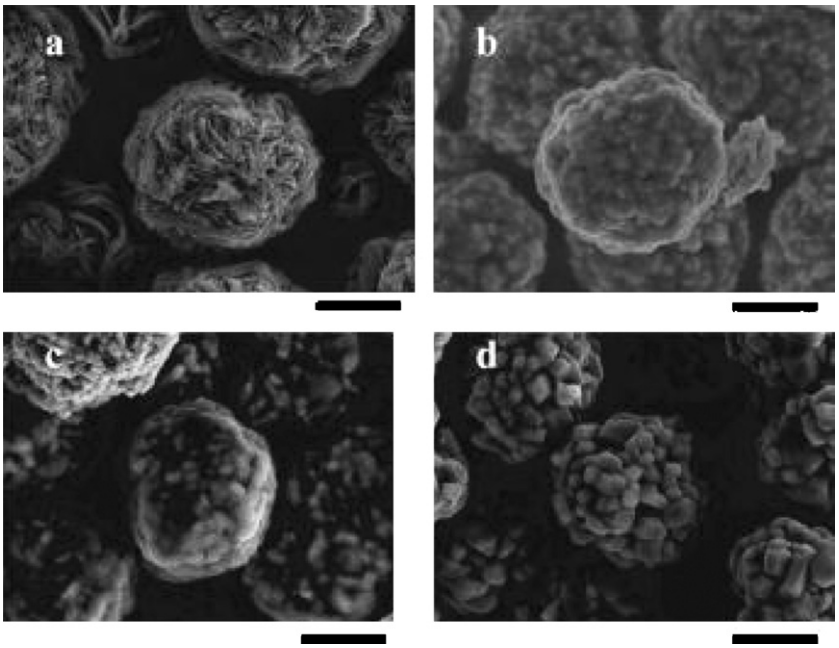

Fig. 3. Scanning electron microscope micrographs showing the morphology change of the (d) $Li[Ni_{1/3}Co_{1/3}Mn_{(1/3-0.04)}Mg_{0.04}]O_{1.96}F_{0.04}$ sample compared to non-fluorinated (c) $Li[Ni_{1/3}Co_{1/3}Mn_{(1/3-0.04)}Mg_{0.04}]O_2$, (b) Li $[Ni_{1/3}Co_{1/3}Mn_{1/3}]O_2$ and (a) $Li[Ni_{1/3}Co_{1/3}Mn_{1/3}](OH)_x$ samples. The samples were fabricated by co-precipitation followed by heat-treatments at elevated temperature. The scale bar indicates 5 μm [22].

addition, $LiCoO_2$ [28] fabricated by solid state with up to 5 wt.% LiF demonstrated improved first cycle coulombic efficiency proposed to be induced by increased particle size and crystallinity. The influence of fluorine on the cycling performance of the Li–Ni–Co–Mn compounds was proposed to derive from a combination of features. These include (i) the aforementioned enhanced physical properties, (ii) enhanced cation ordering [22], (iii) improved structural stability associated to the smaller *c*-axis variation during charge and (iv) the presence of fluorine near the surface previously proposed to provide protection from HF attack at high voltage in fluorine-doped spinels [26]. In addition, reduced or negligible cell resistance, based on the differential voltage profiles upon cycling of the F-substituted $LiNi_{1/3}Co_{1/3}Mn_{1/3}O_2$ compounds [20], is consistent with results obtained more recently by impedance spectroscopy suggesting the stabilization of the surface interface with the electrolyte contributed to improved cycling performance [29]. Mn-rich $Li(Li_{0.2-}Ni_{0.15+0.5z}Co_{0.1}Mn_{0.55-0.5z})O_{2-z}F_z$ compounds $(0 \leq z \leq 0.1)$ [30], obtained by sol–gel synthesis using glycolic and tartaric acid as chelating agents followed by a 900 °C heat-treatment [31] also showed improved cycling stability at room and elevated temperatures, and decreased cell impedance with increasing fluorine content for $z < 0.1$.

2.1.1.2. Spinel lithium manganese oxyfluorides. Three-dimensional $LiMn_2O_4$ spinels, which offer cost and environmental advantages, have been proposed as an alternative cathode material to layered transition metal oxides. However, the poor elevated temperature performance initially demonstrated by the spinel materials concerned battery manufacturers despite potential advantages such as improved safety, a critical characteristic for large-scale applications. Driven by the finding that cation substitution (Li, Co, Cr, Mg, Fe) was successful in improving the room temperature cycling of $LiMn_{2-y}M_yO_4$ spinels, the effect of the substitution of fluorine for oxygen on the electrochemical performance of $LiMn_2O_4$ was investigated by Amatucci et al. [32,33]. The lithium manganese oxyfluorides were obtained from stoichiometric mixtures of γ-MnO_2, Li_2CO_3 and LiF. The precursors were heated in air at 800 °C for 24 h followed by a few grinding steps and annealing at the same temperature. Although detrimental when fluorine substitution is utilized alone [32–34], the addition of fluorine concomitant to lithium cation substitution in $Li_{1+x}Mn_{2-x}O_{4-y}F_y$ improved the materials capacity retention after elevated temperature storage by approximately 50% compared to optimized $Li_{1+x}Mn_{2-x}O_4$, while also maintaining good electrochemical performance at room temperature. These oxyfluorides proved to be more resistant to HF attack, which results in manganese dissolution, and its structure more stable after storage at elevated temperature, both of which promoting capacity fade during elevated temperature storage. The higher ionicity of the Mn–F bonds existing in the oxyfluoride spinel may result in Mn^{3+} ions of lower mobility, due to local electronic deprivation, and therefore of lower reactivity towards dissolution. Although the $Li_{1+x}Mn_{2-x}O_{4-z}F_z$ oxyfluoride spinels showed enhanced electrochemical performance, more efforts were required especially towards improving elevated temperature cycling. The authors pursued the search for the most appropriate cation substitutions to stabilize the MO_6 network in an attempt to prevent manganese dissolution since the Mn^{3+} dismutation process involves a rearrangement of the MnO_6 structural. Aluminum substitution, which had been largely disregarded based on coordination considerations, may offer stabilization of

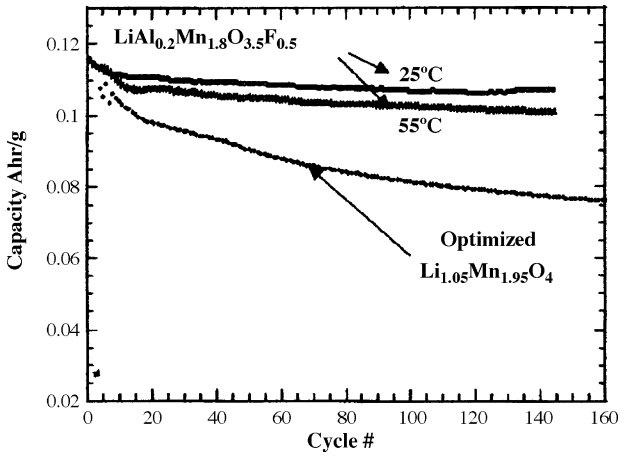

Fig. 4. Discharge capacity as a function of cycle number for $LiAl_{0.2}Mn_{1.8}O_{3.5}F_{0.5}$ at 25 and 55 °C compared to the optimized $Li_{1.05}Mn_{1.95}O_4$ at 55 °C. The cells were cycled vs. lithium metal between 3.5 and 4.3 V at C/5.

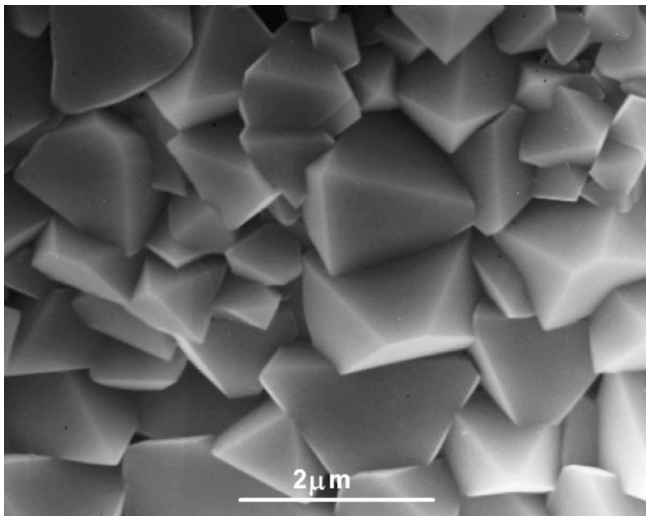

Fig. 5. Field emission scanning electron micrograph showing the morphology of a $Li_{1.05}Mn_{0.95}O_{1.8}F_{0.2}$ sample.

the MO_6 substituted octahedral entity due to its polarizing power associated to its relatively small ionic radius. As expected, the $LiAl_xMn_{2-x}O_{4-z}F_z$ [26,35–37] solid solutions fabricated by solid-state synthesis were found to maintain good room temperature cycling stability while showing improved elevated temperature cycling stability compared to the optimized $Li_{1.05}Mn_{1.95}O_4$, as illustrated in Fig. 4. A link between the room temperature and the elevated temperature failure mechanisms of lithium manganese spinels was established utilizing extensive physiochemical and electrochemical characterization of a mixed sample of spinel materials from the following classes, $L_{1+x}Mn_{2-x}O_4$, $Li_{1+x}Mn_{2-x}O_{4-z}F_z$, $LiAl_xMn_{2-x}O_{4-z}F_z$ and $LiMg_xMn_{2-x}O_{4-z}F_z$ [38,39]. Smaller lattice parameters were found necessary to resist the physical destruction induced by a surface Jahn-Teller distortion associated to the chemical failure exacerbated at elevated temperature. The Al^{3+} substitution resulted in increased quantity of electrochemically inert Mn^{4+} ions and decreased amount of Jahn-Teller but electroactive Mn^{3+} ions. Although favorable to the cycling stability, this was detrimental to the material specific capacity in the absence of fluorine. The concurrent fluorine substitution was carried out to increase the manganese average oxidation state in order to reduce capacity while retaining small lattice size to maintain good cycling stability, both at ambient and elevated temperatures. Various cationic co-substitutions such as Al [35,40], Mg [38,41], Co [32,40], Cr [32,40,42], Fe [32], Ti [43], Ni [43] and Cu [43] and synthesis methods have been considered to improve the spinel materials electrochemical performance with various degrees of success.

Besides the substitutional effect of fluorine, the fluxing effect of LiF is significant as observed with particles of larger size and of well-defined and pronounced grown facets in Fig. 5. These characteristics are consistent with the common use of metal-halogenide fluxes for inorganic crystal growth [44]. The addition of LiF offers the possibility of size and morphology control of the spinel materials. Previous communications had shown the crucial impact of the spinel surface and interface with the liquid electrolyte on the resulting electrochemical performance. $LiAl_xMn_{2-x}O_{4-z}F_z$ exhibited lower resistance to charge transfer during room temperature cycling [45]. In addition, minimization of the interface with electrolyte was demonstrated to benefit elevated temperature storage and room temperature cycling, by lowering the catalytic effects of the spinel towards electrolyte oxidation and manganese dissolution [46]. This was achieved by reducing the spinels surface area (e.g. larger particle size) or by using a method of encapsulating the spinel particles [26,33]. A microwave assisted sol–gel method has been recently developed to synthesize $LiAl_{0.1}Mn_{1.9}O_{3.9}F_{0.1}$ spinel of controlled morphology while reducing the fabrication reaction time [47]. Indeed, uniform and rapid heating had already been achieved using microwave energy for the synthesis of $Li_{1+x}Mn_{2-x}O_{4-y}F_y$ spinels [48].

Finally, the anode material was shown to significantly affect the electrochemical performance of the cell. Improved elevated temperature performance was attained versus lithium metal and spinel $Li_4Ti_5O_{12}$ anodes with the use of $LiAl_xMn_{2-x}O_{4-z}F_z$ solid solution, however capacity fade was still observed when carbonaceous anodes were utilized. Postcycling analyses demonstrated the carbonaceous anode participates in the failure mechanism through the formation/dissolution of its SEI layer sustained by a shuttle mechanism upon cycling [49].

Driven by the positive impact of the Al and F co-substitutions on the electrochemical behavior of spinel $LiMn_2O_4$, the same co-substitutions were applied to a different cubic spinel system, $Li_4Ti_5O_{12}$ [50]. $Li_{4.15}Al_{0.15}Ti_{4.85}F_{0.6}O_{11.4}$ was obtained by solid-state synthesis using TiO_2, Li_2CO_3, Al_2O_3 and LiF precursors heat-treated at 950 °C in air. Unfortunately, in this case, the addition of fluorine deteriorated the material electrochemical performance as observed with the reduction of the reversible capacity and capacity retention compared to the undoped material.

2.1.1.3. Orthorhombic lithium manganese oxyfluorides. The studies of the substitution of fluorine for oxygen described so far were carried out on the two main positive electrode structure

types, layered lithium transition metal oxides and lithium manganese cubic spinels. More recently, the investigation of fluorine substitution was extended to a different structure type, the orthorhombic lithium manganese oxide, $LiMnO_2$ [51]. Orthorhombic $LiMnO_2$ (*o*-$LiMnO_2$) has a large theoretical capacity, 285 mAh/g, but suffers from poor cycling stability at elevated temperature again attributed to the acid-driven dissolution of manganese since the orthorhombic structure transforms into a spinel-like structure upon cycling. As observed previously with lithium manganese spinels $LiMn_2O_4$, the sole addition of fluorine did not help the elevated temperature cycling stability of *o*-$LiMnO_2$. However, the addition of fluorine combined to excess lithium in *o*-$Li_{1.07}Mn_{0.93}O_{1.92}F_{0.08}$ resulted in improved rate capability and capacity retention at elevated temperature. These phenomena were correlated to the well-defined crystallinity of the oxyfluorides and to a reduced amount of stacking faults in comparison to the undoped *o*-$LiMnO_2$ compound. The existence of stacking faults of local monoclinic arrangement due to cation mixing were proposed to facilitate the detrimental transition of the initial orthorhombic into the spinel-like structure resulting in capacity fade at elevated temperature.

2.1.2. Surface fluorination

In this section, we report on the investigation of the influence of surface fluorination on the electrochemical properties of intercalation compounds. This is in contrast to the bulk substitution described above. As the transport of both lithium and electron occurs at the surface of the active material, surface properties including chemistry are expected to have a strong impact on the active materials electrochemical performance. Studies on the surface fluorination of both lithium transition metal cathode materials and carbonaceous anode materials will be presented.

In the case of intercalation in cathode materials, the presence of surface fluorine is expected to improve electrochemical performance by: (1) facilitating the lithium ion solvation/desolvation processes, (2) increasing surface electric conductivity, (3) reducing electrolyte oxidation, (4) stabilizing the surface structure upon cycling and finally (5) shielding the active material from HF attack [52]. Surface fluorination of $LiCoO_2$, $LiNiO_2$, $LiNi_xCo_{1-x}O_2$ and $LiMn_2O_4$, was considered by Takashima and coworkers [53,54]. Surface fluorination was performed by reaction with a gaseous fluorinating reagent such as elemental fluorine F_2, ClF_3 and NF_3. Controlled surface fluorination can improve electrochemical performance such as discharge capacity, average discharge capacity, cycling efficiency and cycling stability. Fluorination conditions (including temperature, fluorinating agent chemistry and pressure) influence the materials electrochemical behavior. In the case of $LiMn_2O_4$, better results were obtained with F_2 [55] than with NF_3 [56] as fluorination agent. Higher temperatures promoted fluorination towards the core of the materials, as illustrated by the XPS spectra of the F 1s level of $LiCoO_2$ fluorinated with NF_3 and ClF_3 in Fig. 6. However, excess fluorination was found to deteriorate performance due to the formation of resistive fluoride-based surface films. The authors also proposed the addition of a carbon coating in combination with fluorination [52,57]. The arrangement of the carbon and fluorine or fluoride-based layers appears to directly affect the electrode properties. The material obtained by deposition of the carbon film following fluorination exhibited lower capacity loss over 50 cycles with respect to the materials modified by fluorination alone or performed after carbon

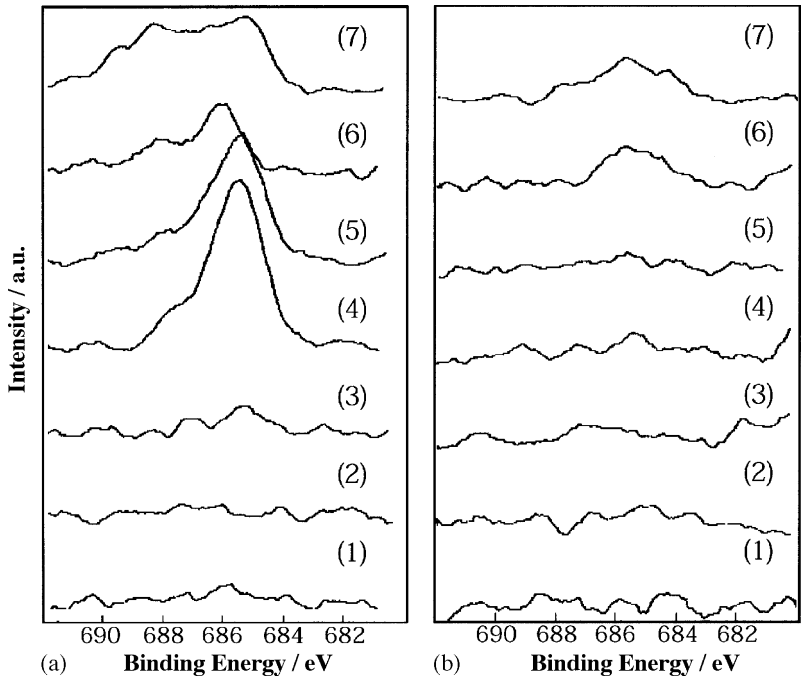

Fig. 6. XPS spectra of F 1s level in $LiCoO_2$ treated with NF_3 and ClF_3 at 1.3 kPa (a) before and (b) after argon sputtering for 30 min. (1) Untreated, (2) NF_3 at RT, (3) NF_3 at 100 °C, (4) NF_3 at 200 °C, (5) NF_3 at 500 °C, (6) ClF_3 at RT and (7) ClF_3 at 100 °C [52].

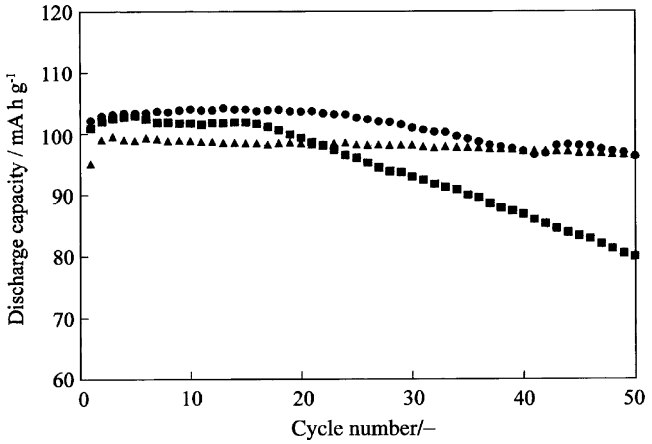

Fig. 7. Discharge capacity plotted as a function of cycle number for (●) $LiMn_2O_4$ submitted to fluorination alone, (▲) $LiMn_2O_4$ submitted to fluorination followed by a carbon treatment and (■) $LiMn_2O_4$ submitted to a carbon treatment followed by fluorination. The $LiMn_2O_4$ samples were cycled vs. lithium metal between 3.4 and 4.3 V at a 0.3C rate [52].

coating (Fig. 7). The carbon film was proposed to protect the surface fluorine introduced during fluorination from being removed during cycling.

In search for cathode materials of higher capacity, metal oxide coatings have been developed to improve the cycling performance of $LiCoO_2$ materials charged above 4.2 V. More recently, Sun et al. [58] revealed metal fluorides can also form efficient surface coatings. AlF_3 coatings demonstrated improved cycling performance and rate capability, with no sacrifice in the initial reversible capacity (Fig. 8). These results were attributed to lower charge transfer resistance and reduced Co dissolution. The AlF_3 coating was proposed to reduce surface LiF formation, responsible for impedance increase, and to efficiently protect the active material from HF attack contributing to detrimental cobalt dissolution.

Surface fluorination was also utilized to modify the electrochemical properties of carbonaceous materials, such as natural graphites, petroleum cokes and pyrocarbon, used as negative electrode in Li-ion cells. Surface modification of

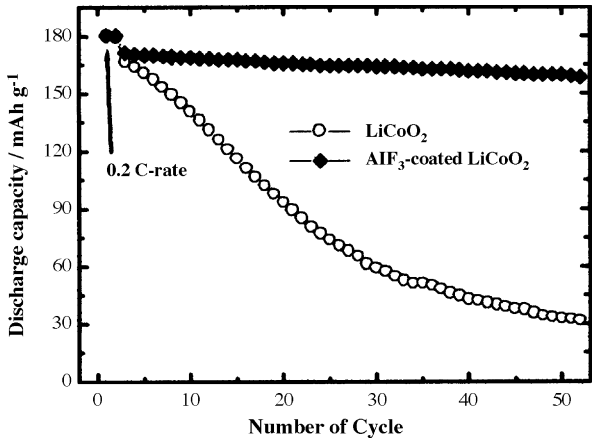

Fig. 8. Discharge capacity as a function of cycle number for AlF_3-coated $LiCoO_2$ compared to pristine $LiCoO_2$ cycled vs. lithium metal between 3 and 4.5 V under a constant current of 20 mA/g [58].

natural graphites, performed by chemical fluorination using elemental fluorine [59–63] between 150 and 300 °C and by radiofrequency plasma fluorination using CF_4 [61,62,64], resulted in capacities slightly exceeding the theoretical 372 mAh/g value. The main advantage of these fluorination treatments is that they increase the capacities of natural graphites with no sacrifice in the material's coulombic efficiencies, or even in some cases with slightly improved coulombic efficiencies. Increased surface area, larger volume of smaller surface mesopores and increased surface disorder (Fig. 9) caused by partial C–C bond breaking were reported to allow the storage of larger amounts of lithium ions. Surface chemistry is also a critical feature to control performance. Lower amounts of hydrogen and oxygen exist on the surface of graphite fluorinated with elemental F_2 at 200 and 300 °C compared to non-treated samples. Surface hydrogen had been previously reported to cause large charge–discharge hysterisis [65] while oxygen increased first cycle irreversible capacity loss [66–68]. Finally, a more recent approach consisted in the fluorination of natural graphite using ClF_3 [69].

Surface fluorination using elemental fluorine was also applied to petroleum cokes [62,70–73]. The fluorine modification

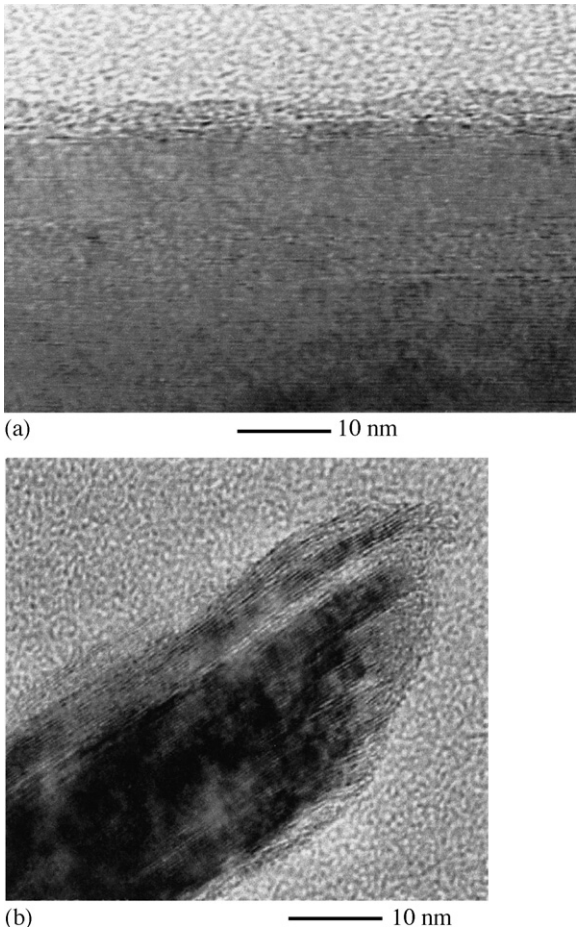

Fig. 9. Transmission electron micrographs showing the disordered structure of the surface fluorinated layers compared to the graphene layers of the core. (a) A 25 μm average size graphite was treated with elemental fluorine at 250 °C. (b) A 40 μm average size graphite was treated with elemental fluorine at 300 °C [62].

slightly reduced discharge capacities but significantly improved first cycle coulombic efficiencies. Although fluorine treatment did not affect the surface area significantly, the opening of surface closed edges, the increased surface disorder and surface defects were proposed to facilitate the accommodation of lithium ions, while the presence of decreased surface oxygen was proposed to have a positive effect on coulombic efficiency.

Finally, the electrochemical properties of pyrocarbon were also improved by surface fluorination using NF_3 [74,75]. The highest performance was obtained for fluorination performed at 400 °C with a 7% capacity increase and enhanced coulombic efficiency.

2.2. Fluorophosphates

Phosphate polyanion-based materials such as $LiFePO_4$ have shown good electrochemical performance as positive electrode materials for Li-ion batteries. Of particular interest is the higher thermal stability of the phosphate framework, crucial characteristic to improve battery safety, especially for large cells. In addition, the high electronegativity of fluorine raised interest in fluorides as positive electrode materials. The latter being higher than the one observed for oxygen, higher intercalation voltages can be expected using the same $M^{n+}/M^{(n+1)+}$ redox reaction. Fluorophosphates can therefore appear as a promising class of materials if one wants to combine these two desirable characteristics.

The $AMPO_4F$ compounds, where A is Li or Na and M is a 3d transition metal, were the first fluorophosphates recognized as alkali ion insertion hosts [76]. The vanadium-based materials, $LiVPO_4F$ and $NaVPO_4F$, synthesized by a two-step carbothermal reduction process, were evaluated for their electrochemical properties versus lithium metal [77]. The initial attempts at the $LiVPO_4F$ synthesis resulted in a reversible capacity close to 120 mAh/g. However, after optimization of the fabrication process, improved reversibility and room temperature cycling stability were attained with a discharge capacity close to the 155 mAh/g theoretical capacity at a C/15 rate between 3 and 4.5 V [78,79]. The material was also evaluated in a Li-ion cell configuration utilizing a graphite anode. $LiVPO_4F$ delivered a 123 mAh/g reversible capacity at an average discharge voltage of 4.06 V, while maintaining good capacity retention over 300 cycles between 3 and 4.4 V at a 1C rate [78,79]. Based on these results, $LiVPO_4F$ offers a 0.3 V greater discharge voltage and a flatter voltage profile compared to the state of the art $LiCoO_2$ system, showing the potential of this lithium phosphate system as positive electrode material for Li-ion cells. The high discharge voltage of $LiVPO_4F$ was attributed in a previous communication [80] to the presence of fluorine in the $LiVPO_4F$ structure. Indeed, compared to phosphates compounds such as $Li_3V_2(PO_4)_3$ and $VOPO_4$ utilizing the same V^{3+}/V^{4+} redox couple as $LiVPO_4F$, the latter revealed a 0.3 V lithium intercalation voltage increase. Finally, a symmetrical $LiVPO_4F$ Li-ion cell with an average discharge voltage of 2.4 V was proposed based on the reversible reactions observed at 1.8 and at 4.2 V versus lithium [81].

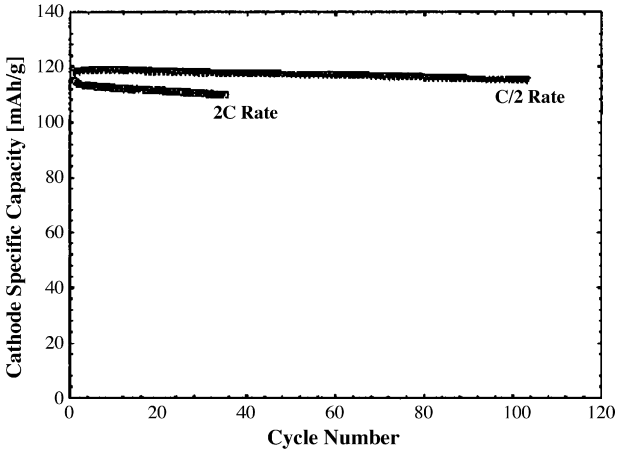

Fig. 10. Specific capacity as a function of cycle number for $Na_3V_2(PO_4)_2F_3$ cycled vs. graphite between 3 and 4.6 V at C/2 and 2C rates using a 1 M $LiPF_6$ in EC-DMC (2:1 by weight) electrolyte [83].

The sodium-based fluorophosphate $NaVPO_4F$ was analyzed in a lithium metal cell configuration [77]. In this configuration, sodium ions are extracted from the $NaVPO_4F$ framework in the first charge, plated on the lithium anode and replaced for lithium ions in the following discharge. $NaVPO_4F$ delivered reasonable initial reversible capacity, 110 mAh/g, and good cycling stability both at room temperature and 60 °C, upon cycling between 3 and 4.5 V. In addition to interesting performances in lithium-based applications, $NaVPO_4F$ was identified as potential positive electrode material for sodium ion batteries utilizing hard carbon anodes, as it was found to react with sodium reversibly [82].

The authors pursued the investigation of sodium-based fluorophospate materials and developed a hybrid-ion cell utilizing a graphite anode, a sodium insertion cathode, $Na_3V_2(PO_4)_2F_3$, and a $LiPF_6$-based electrolyte [83]. Preliminary results showed the graphite/$Na_3V_2(PO_4)_2F_3$ system revealed good cycling stability at a C/2 rate over 100 cycles and initial cathode specific capacity close to 120 mAh/g (Fig. 10). Although sodium ions are extracted in the first charge from the fluorophosphate structure into the electrolyte, the reaction mechanism occurring upon subsequent cycling is still unclear although it most probably involves the reversible intercalation of lithium ions into the initially sodium-based cathode structure. The main shortcoming of this type of system consists in the fact that the source of lithium is strictly limited to the $LiPF_6$-based electrolyte, which may require excess electrolyte to allow full utilization of the electrode materials.

A second class of fluorophosphates, Li_2MPO_4F (M = Ni and Co), of higher operation voltage ($\geq$5 V) and larger theoretical capacity (310 mAh/g) (if $2Li^+$ can be reversibly removed) has been found to exhibit interesting electrochemical properties. Okada et al. [84] reported preliminary results confirming the reaction of Li_2CoPO_4F with lithium proceeds at 5 V utilizing a 1 M $LiPF_6$ in ethyl methyl sulfone electrolyte (Fig. 11). Li_2CoPO_4F also revealed lower metal dissolution during storage in a 1 M $LiPF_6$ ethyl carbonate–dimethyl carbonate

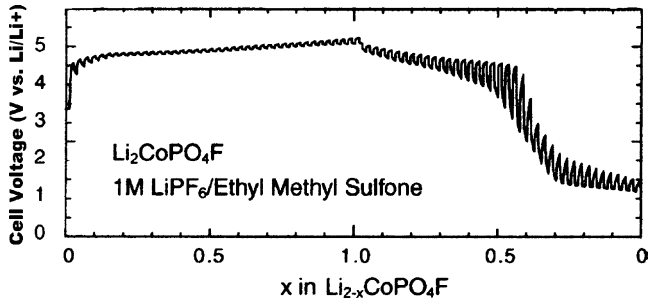

Fig. 11. Quasi-open circuit voltage profile for Li_2CoPO_4F cycled vs. lithium metal [84].

(1:1) electrolyte, both at room and elevated temperatures, and higher thermal stability in the charged state than the more conventional $LiCoO_2$ and $LiMn_2O_4$ cathode materials. Similar results were expected with the Li_2NiPO_4F compound. However, the electrochemical testing of Li_2NiPO_4F attempted utilizing the same sulfone-based electrolyte remained unsuccessful most certainly due to electrolyte instability. The Li_2NiPO_4F open circuit voltage value was estimated at 5.1 V by calculation [85].

2.3. $LiAMF_6$ fluorides

First principle band-structure calculations were utilized to predict the lithium intercalation voltage of $LiCaCoF_6$ and $LiCdCoF_6$ [86]. Although these $LiAMF_6$ compounds, with formal charges of 2^+ and 3^+ for A and M, respectively, utilize the same Co^{3+}/Co^{4+} redox reaction as that of $LiCoO_2$, the calculated intercalation voltage was 2 V higher with a value of approximately 6 V. Small theoretical volume changes, estimated to be below 3% upon delithiation, also suggest promising structural stability upon cycling. Although the $LiAMF_6$ compounds exhibit different structures, the local atomic arrangement around M and F and therefore the electronic structure, mainly determined by chemistry and coordination, may not vary significantly. The variety of choice for A and M in $LiAMF_6$ was proposed to offer the possibility to optimize other crucial properties such as lithium diffusion and chemical stability, while maintaining the advantage of high intercalation voltage. However, oxidation resistant electrolytes for operation up to 6 V must be developed in order to evaluate experimentally the electrochemical properties of this new type of electrode materials.

3. Carbon fluorides

The low equivalent weight and high theoretical output voltage of carbon fluorides make them one of the most theoretically favorable materials for high specific energy batteries. Most carbon fluoride materials offer exceptional stability and very low self discharge. As opposed to the intercalation based reactions discussed above for the transition metal oxyfluorides, the carbon fluorides operate on a displacement or conversion reaction where the carbon fluorides are decomposed to carbon and lithium fluoride upon cathodic discharge (1).

$$Li^+ + CF_x \rightarrow xLiF + C \quad (1)$$

Carbon fluorides can be classified in two main categories, high temperature (HT) fabricated graphite fluorides consisting of $(CF)_n$ (first-stage) and $(C_2F)_n$ (second stage) compounds [87], and low temperature (LT) fabricated fluorine-graphite intercalation compounds of CF_x. While the HT graphite fluorides are covalently bonded, the CF bonds of the LT compounds exhibit a more ionic character. The HT CF compounds are usually fabricated from various carbon and graphite precursors at a relatively high temperature of 400–600 °C in fluorine atmosphere to induce the fluorination reaction. At much lower temperatures, the more ionic LT CF_x compounds are formed using various Lewis acids as oxidation aids. The carbon bonding remains very much sp^2 in LT CF_x compounds and various degrees of staging occur among the graphene layers as the fluoride anion intercalates between the basal planes of the graphene sheets. Due to its ionic character, the LT CF_x compounds retain very good electronic conductivity and are black in color. These materials are in sharp contrast to the covalently bonded graphite fluorides $(CF)_n$ and $(C_2F)_n$ that are white to light grey in color and are quite insulating. Fabrication of these materials greatly disrupts the precursor structure to induce the formation of puckered graphene planes. In the case of $(C_2F)_n$ the proposed structure is very much diamond-like. These layers are sp^3 bonded (trans linked cyclohexane chairs) and the fluorine atoms are covalently bonded to carbon leading to exceptional chemical stability (Fig. 12) [88]. This compound can be classified as a graphite fluoride polymer.

3.1. HT $(C_xF)_n$

Due to the high fluorine to carbon ratio, the covalently bonded $(CF)_n$ graphite fluorides have traditionally been the

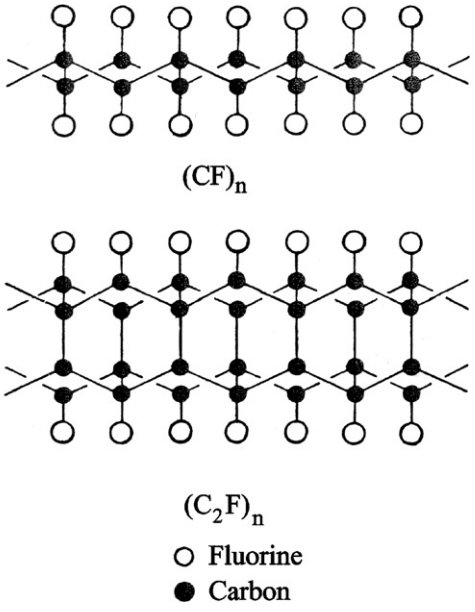

Fig. 12. Schematic showing the structure of a monolayer of $(CF)_n$ and $(C_2F)_n$ HT graphite fluorides [88].

most popular carbon fluoride cathode materials utilized for lithium batteries. These materials, as opposed to the LT CF_x materials that will be discussed below, can be fabricated from almost any carbon precursor by reaction in F_2 atmosphere at temperatures ranging from 400 to 600 °C. The optimum temperature is highly dependent on the carbon precursor [89]. The discharge voltage is between 3 and 2 V and the specific capacity for CF_1 is 864 mAh/g. This leads to an approximately 300% increase in energy density over MnO_2, another popular primary cathode material for Li batteries which operates on an intercalation process. The overpotential of the discharge reaction has been correlated to the interlayer spacing $d(0\,0\,1)$ of the graphite fluoride where lower overpotential was recorded for an increase in $d(0\,0\,1)$. The interlayer spacing itself has been shown to be highly dependant on the precursor utilized for the fabrication of $(CF)_n$ [90].

There are two attractive covalently bonded HT CF materials for lithium batteries, the $(C_2F)_n$ compounds and also $(CF)_n$ (Fig. 12). $(CF)_n$ has been the traditional cathode of choice because of its high energy density as noted above. However the development of $(C_2F)_n$ resulted in carbon fluorides of much higher production yields. This material is typically fabricated at the lower temperatures of 375–400 °C for long period of time under flowing fluorine gas. While the theoretical specific capacity of $(CF)_n$ is 864 mAh/g, the theoretical specific capacity of $(C_2F)_n$ is 638 mAh/g due to the decrease in F:C content. This is offset in practical use as the overpotential of $(C_2F)_n$ is approximately 0.4 V less than $(CF)_n$ at moderate current densities. This translates to a higher average discharge voltage thereby making the energy density (Wh/kg) approximately similar under high rate of discharge conditions [91].

Despite the enormous energy density, the covalent $(CF)_n$ compounds have electrochemical performance challenges originating from their insulating character and reaction mechanism. The conversion mechanism generates an insulating LiF product and considerable volume change. Although a poor conductor, during discharge the electronic charge transfer becomes improved due to the fact that although one of the products of the conversion reaction is the insulating LiF, the other product is highly conductive carbon. In some cases, the rate capability of the CF materials can be improved if the insulating LiF product is able to dissolve in the electrolyte [92].

The actual mechanism of the conversion reaction has been open to some debate. Most agree that, to a certain degree, lithium ions enter the carbon fluoride solvated with the nonaqueous electrolyte solvent. This results in the formation of a transient compound of Li^+(solvent)CF. This compound then spontaneously decomposes to C + LiF + solvent (Fig. 13) [93,94]. The formation of the Li_xCF solid solution and variations of this mechanism has been ascribed as the reason for the experimental OCV of CF compounds (3–3.5 V) being more than 1 V below that of the thermodynamically calculated value of 4.5 V [95,96]. The OCV of covalently bonded CF_x compounds are typically considerably lower than their ionic counterparts, which will be discussed next, due to the stronger covalent bonding. Although the average voltage of the covalent graphite fluorides is lower than the more ionic compounds, they exhibit higher energy density. At low discharge rates, the voltage decrease is usually offset by the increase in specific capacity brought about by higher fluorine contents.

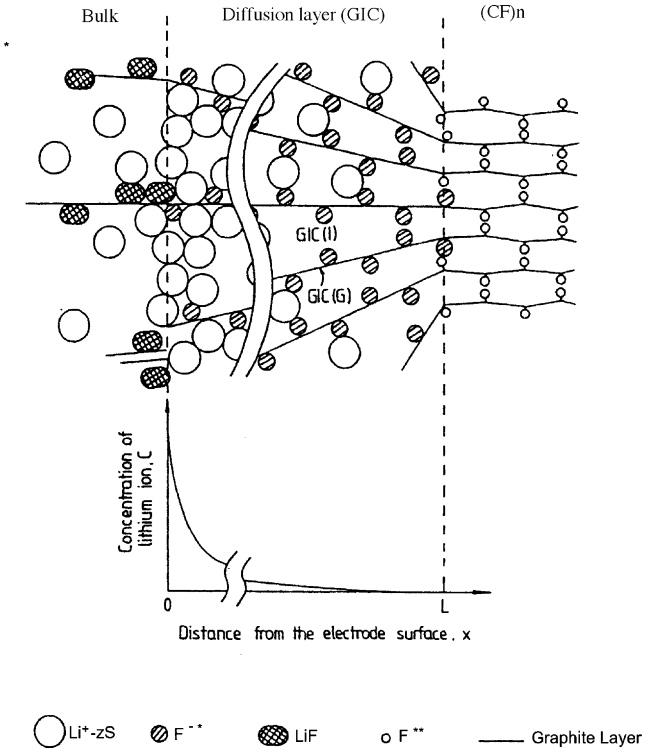

Fig. 13. Schematic of the proposed discharge reaction for the $(CF)_n$ electrode. F^{-*} designates F which is semi-ionically bonded to sp^2 carbons and F^{**} those which are bonded covalently to sp^3 carbon. Li^+-zS corresponds to lithium ions solvated by the nonaqueous electrolyte solvent leading to cointercalation of the graphite fluoride structure [94].

3.2. LT CF_x

The aforementioned use of Lewis acids to induce the fluorination of graphitic precursors at low temperatures has opened a newer area of research in the so-called LT CF_x compounds. These materials contain C–F bonds of ionic character and the carbon retains planar graphitic like structure of sp^2 bonding. Much of the research attention on these materials has been focused on the influence of residual acids in the structure, especially for the acids of HF and IF_5. A detailed structural study was accomplished with the compound $CF_xI_yH_z$ fabricated through the reaction of graphite in a F_2, HF, and IF_5 mixture at room temperature. This product has been post annealed at various temperatures in a F_2 atmosphere. Gradual fluorination occurred through the exchange of IF_x species with F. Systematic fluorination from $CF_{0.72}$ to a high fluorine content of $CF_{0.92}$ was accomplished depending on the temperatures utilized [97]. Although high fluorine contents can be obtained with the IF_5 assisted process, considerable care needs to be undertaken as residual amounts of IF_x can lead to poor self discharge characteristics of the electrochemical cell and lead to poor shelf life performance [98].

As with IF_5, when CF_x materials are synthesized in the presence of anhydrous HF (*a*HF), a degree of HF may be left

intercalated within graphite. The main reason for this is that the fluorination process occurs through an intermediate of $C(HF_2^-)_x$. Polyfluoride species HF_2^- have facile transport within graphite. During the fluorination process, a degree of desolvation occurs releasing HF and resulting in the fluorination of the graphite. At this time, residual HF species may be entrapped within the structure and vacuum pumping is required to isolate the highest purity compounds. If desired, considerable amounts of HF can be accrued within the graphite structure thereby approaching compositions of $C_{3.7}F(HF)_{1.2}$. Such compositions were obtained by the treatment of graphite with elemental fluorine and an oxidant such as K_2PdF_6 in *a*HF [99–101]. Detailed electrochemical investigations have concluded that the presence of HF_2^- in the graphite impedes the conversion reaction during reduction and leads to poor utilization of the electrode material at higher rates. This was explained by a weak interaction between Li^+ and HF_2^- offsetting the conversions brought about by the Li^+ and F^- interaction.

As discussed above, the ionic LT CF_x compounds usually exhibit lower specific capacities due to the lower fluorine contents, but at the same time offer higher average voltages as a result of the ionic bonding, and much improved transport properties relative to the covalently bonded $(CF)_n$. The latter can lead to higher realized specific energy at higher rates of discharge. Fig. 14 portrays this relationship for a variety of LT ionic CF_xs prepared by an IF_5 assisted RT fluorination in HF [102]. The systematic decrease in discharge voltage is shown as a function of post anneal temperature and increasing degree of covalency and fluorine content [103,104].

Reversibility is not well known in the CF_x compounds. However, Yazami and Hamwi [103] has compared the behavior of covalent and ionic CF_x compounds using cyclic voltammetry. This was performed utilizing solid polymer electrolytes to avoid any solvent cointercalation. The covalent HT $(CF)_n$ compound showed no evidence of reversibility. Conversely, the ionic CF_x compounds displayed evidence of reversibility with two small reversible bands at approximately 3 V. In general some degree of reversibility was shown for all the LT CF_x compounds post annealed below 450 °C, well in the sp^2 hybridization. However, no accounting of the actual reversible specific capacity has been given.

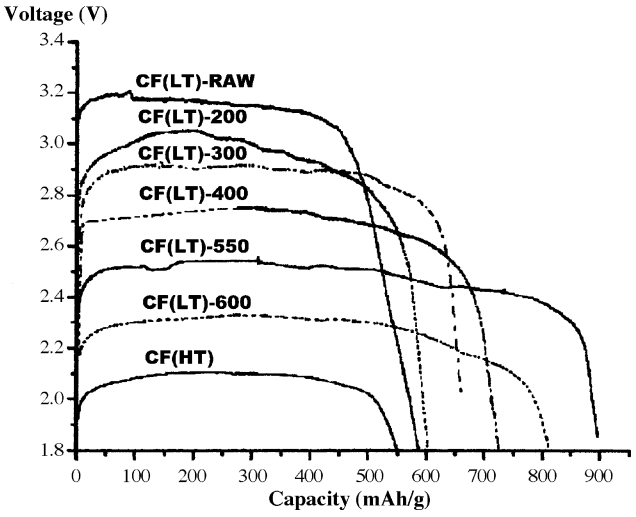

Fig. 14. Discharge profiles of various LT(CF_x) materials as a function of their fabrication temperature, resulting fluorine content, and covalency compared with a purely covalent HT $(CF)_n$ material. Cells were discharged at a rate of 10 mA/g vs. Li metal as negative electrode in 1 M $LiClO_4$ propylene carbonate electrolyte [102].

In contrast to graphites which require the presence of additional oxidants during synthesis, fullerenes react readily with gaseous fluorine at room temperature. Fullerenes have been investigated as they easily form graphite fluorides with relatively high fluorine content (such as $C_{60}F_{46–54}$ [105,106] and $C_{70}F_{52–56}$ [107]) [108]. The higher fluorine content fullerenes were derived from higher temperature reactions approaching 300 °C and were much more crystallized than the lower fluorine content counterpart. Temperatures are kept below 300 °C as the cage structure of the C_{60} and C_{70} has a tendency to rupture at temperatures higher than 300 °C [107]. Fluorination through wide range of $C_{60}F_x$ contents to a fully fluorinated covalently bonded white $C_{60}F_{60}$ has been accomplished at the very low temperatures of 70 °C for 12 days in fluorine atmosphere [109]. Despite this synthesis breakthrough, the fluorinated fullerenes have a tendency to dissolve in the commonly utilized electrolyte solvents which has severely limited their practical applicability. However, application of the fluorinated fullerenes to solid polymer electrolyte systems has greatly reduced this problem where near theoretical capacities have been identified at slow rates with higher OCV than graphite fluorides [110]. In the previous referenced study, it was demonstrated that the reaction of the fluorinated fullerene with Li proceeds as a homogeneous 2-phase reaction (2) with continuously decreasing F/C ratios in the $C_{60}F_x$ during discharge. This is in sharp contrast to the heterogeneous reaction shown for the majority of the graphite fluorides (3) where the C/F ratio remains the same throughout the discharge process in a 3-phase reaction.

$$C_{60}F_x + nLi^+ \rightarrow C_{60}F_{x-n} + nLiF \quad (2)$$

$$CF_x + nLi^+ \rightarrow (1-n)CF_x + nC + nLiF \quad (3)$$

Outside the solid polymer electrolyte approach, the use of C_{60} versus C_{70} based fluorinated fullerenes has shown improved behavior in liquid electrolytes by granting both improved stability to dissolution and specific capacity [108,111].

3.3. Graphite fluoride oxide

Graphite has been known to form poorly defined graphite oxide compositions for many decades. These are typically obtained through the oxidation of graphite by strong oxidizers such as HNO_3 and $KClO_3$. Ideally, the formula for graphite oxide is C_4OOH but many compositional variations occur depending on fabrication and ambient storage conditions. Due to the decrease in anion electronegativity, the discharge reaction of graphite oxides is typically around 2 V versus the 2.5–3.4 V of graphite fluorides. Subsequently, there has been a quest to synthesize and characterize the electrochemical

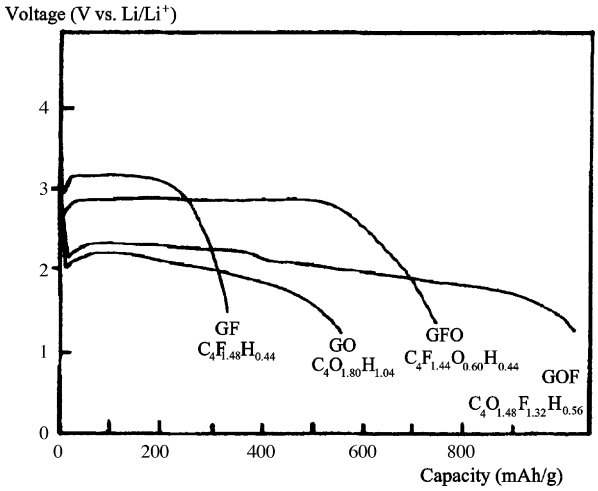

Fig. 15. Galvanostatic discharge of various LT graphite fluorides, oxyfluorides and oxides. Testing was performed at 0.025 mA/cm^2 vs. Li metal in 1 M $LiClO_4$ propylene carbonate electrolyte [108].

properties of graphite oxide fluorides. Synthesis of these materials was attempted from various methodologies. Most consisted of the fluorination of graphite oxides. The fluorination through the use of fluorine gas [112,113] or BrF_3 [114] was demonstrated at relatively low temperatures. Conversely, an alternative method consisted in the fabrication of a LT CF_x through the method of F_2, HF and IF_5 mixture then oxidizing the resulting LT CF_x through the use of HNO_3 and other oxidizers [115]. The electrochemical properties of the graphite oxide fluorides were a composite of the graphite fluorides and graphite oxides (Fig. 15). This trend in output voltage profile tracked systematically with the degree of ionicity induced by the F to O ratio. The C–F bonds in oxygen rich oxyfluorides were more covalent versus the more ionic bonding identified in the fluorine rich materials.

3.4. Carbon metal fluoride intercalation compounds

As previously noted, the use of various MeF_x species as oxidizing aids to the intercalation of F^- into graphites to form LT CF_x resulted in the formation of graphite fluorides with residual MeF_x species remaining in the interlayer (i.e. $CF_x(MeF_y)_z$). For the most part, these were considered impurities. However, when the oxidant is a metal fluoride, especially a 1st or 2nd row transition metal, this offers a unique opportunity to form new cathode materials. Although investigated for an array of compounds, this concept is usually limited due to the low MeF_x to C ratio, thereby resulting in a low % of active material by weight and volume. In spite of this, there are a few new developments in this area worth mention on the basis of synthesis. As discussed above C_{60} fullerenes have been shown to be quite reactive with metal fluoride gasses. In particular, $C_{60}(MoF_6)_9$ and $C_{60}(IrF_6)_{19}$ have been isolated [116]. In general, it has been found that although Lewis acidity is important, the fact remains that the intercalation of the metal fluoride species will not occur unless the oxidation power is strong enough to oxidize the carbon host. In that spirit, Hamwi and Claves has also recently described the intercalation of NbF_5, TaF_5, and TiF_4 into the C_{60} lattice [117]. Impact on energy storage relative to graphite fluorides is questionable at this time. Through the oxidation of second stage MeF_n-GIC (graphite intercalation compound) by hexamethyldisiloxane, unique second stage Nb, W, and Mo oxyfluoride GICs were fabricated. In addition, third stage V and Cr/V oxyfluoride GICs were stabilized [118]. Various degrees of reduction capacity were noted when tested in lithium metal batteries. Some reversibility is noted but the capacity realized may be partly due to the intercalation of ClO_4^- electrolyte salt upon the anodic recharge sweep.

3.5. Graphite fluorides characterization

As with all fluorides and oxyfluorides, the characterization of structure and the degree of ionicity of the C–F bonds is necessary for the development of accurate models to explain electrochemical behavior. X-ray diffraction remains the classical useful technique for characterizing structural aspects. The (0 0 l) reflections give the *d*-spacings between the layers and aid in the identification of complex anion species depending on their steric effects on lattice expansion. In addition, these planes give direct account of the staging of the intercalate in the graphite intercalation compounds. Systematic characterization of the ionicity of the C–F bond can also be inferred through the calculation of the C–C bond distance. In the case of LT ionic sp^2 CF_x materials the C–C bond distance is approximately 1.42 Å, as the degree of covalent CF_x develops, the C–C bond distance approaches that of pure sp^3 carbon value of 1.48 Å. Sharp contrasts also develop in FTIR data. Covalent C–F bonding shows strongly in the 1216 cm^{-1} region while semi-ionic bands can range in the region from 1127 to 1148 cm^{-1}. Finer detail can be extracted from the use of EPR and NMR. ^{19}F NMR clearly shows the significant shifts as the CF bond transitions from ionic to covalent.

4. Metal fluorides

Evolving from the discussion of carbons intercalated with metal fluoride anions, we open a review of the metal fluorides themselves as cathode materials for lithium batteries. The obvious advantage relative to the carbon rich carbon metal fluoride is that there is a much improved efficiency due to the lack of extreme ratios of excess carbon.

4.1. Primary lithium batteries

Based on thermodynamic calculations, the theoretical energy density of the conversion reactions (4) occurring with metal fluorides exceeds that one would expect for metal oxides and sulfides due to the much higher average voltage (Table 1). The majority of this improvement is due to the highly ionic character of the metal fluoride bond brought about by the electronegativity of F relative to the covalent characteristics of the dichalcogenide Me–O and Me–S bonds. It is for this reason that metal fluorides were looked at quite intensively in the late

Table 1
Theoretical average voltage, specific capacity, and specific energy expected during a conversion reaction with Li for a variety of divalent and trivalent dichalcogenides and fluorides

$Me^{2+}X$	V	mAh/g	Wh/kg
$2Li^+ + Me^{2+}X_z \rightarrow z(Li_{2/z}X) + Me$			
MnF_2	1.92	577	1108
MnO	1.03	756	779
MnS	1.144	616	705
FeF_2	2.66	571	1519
FeO	1.61	746	1201
FeS	1.75	610	1068
CoF_2	2.854	553	1578
CoO	1.8	715	1287
NiF_2	2.96	554	1640
NiO	1.95	718	1400
CuF_2	3.55	528	1874
CuO	2.25	674	1517
CuS	2	561	1122
$3Li^+ + Me^{3+}X_z \rightarrow z(Li_{3/z}X) + Me$			
VF_3	1.86	745	1386
V_2O_3	0.945	1073	1014
CrF_3	2.28	738	1683
Cr_2O_3	1.09	1058	1153
MnF_3	2.65	719	1905
Mn_2O_3	1.43	1018	1455
FeF_3	2.74	712	1951
Fe_2O_3	1.63	1007	1641
BiF_3	3.13	302	945
Bi_2O_3	2.17	345	749

Note the average voltage difference between fluorides and dichalcogenides, and the increasing average voltage with atomic number for the 3d metals.

1960s and very early 1970s as potential cathode materials for lithium batteries.

$$Li^+ + MeF_n \rightarrow {}_nLiF + Me \quad (4)$$

One of the highest energy density cathode materials is CuF_2. This material system was investigated widely in the late 1960s and early 1970s because of this exceptional energy density. Much of the early work focused on CuF_2 with hydrated impurities such as the presence of CuOHF and $CuF_2{\cdot}2H_2O$. Addition of water doping to the electrolyte raised the average voltage, however cells were seen to deliver only 25% of the theoretical energy density [119]. The explanation for the former may be rooted in localized dissolution of the cathode such that it acts as a dissolved cathode which precipitates product upon the reduction reaction. The poor utilization of most fluorides, which will be mentioned routinely in this section, resides in the high electronic resistance of the material brought about by their intrinsically high band gaps. Two strong early efforts to develop usable CuF_2 were brought forth by Globe-Union Inc. [120] and Livingston Electric Corp. [121]. As discussed above, extensive solubility of the hydrated CuF_2 leads to acceptable rate capability and in some cases good utilization, but this was tied with very poor stability. More importantly, voltage profiles were on the order of 2 V instead of the approximately 3 V expected through thermodynamic calculations. The Globe-Union work examined the use of CuF_2 electrode materials synthesized through various techniques to produce CuF_2 electrodes of better utilization. CuF_2 electrodes were formed through sintering CuF_2 on metal current collectors, and electrodeposition of CuF_2 thin films from HF solutions. Although a few of the techniques resulted in appreciable energy densities, all voltages were low. Questions remained regarding the dissolution of CuF_2, the formation of complex oxide based reactions at lower voltages, and the recurring problem of very poor intrinsic electronic conductivity brought about by the high band gap metal fluorides. Although much work was done in this time period, the theoretical utilization of the metal fluorides was never really approached unless a partial dissolution of the electrode was involved [122]. In this case, the cell exhibited poor stability. After two decades of little or no activity on CuF_2, Badway et al. have reported the >90% utilization of CuF_2 at theoretical voltages for the first time [123,124]. This result was enabled through the use of nanosized CuF_2 domains embedded in a matrix of metal oxide or sulfide mixed conductors. The use of CuF_2 nanodomains drastically decreased the electron transport difficulties and increased the effective current capability. The matrix ensured fast lithium and electron transport to the individual nanograins. The best performance was shown for a nanocomposite consisting of MoO_3 based matrices. Although nanocomposites containing carbon matrices were shown to improve the utilization of CuF_2 significantly at a C/40 rate at 22 °C, the use of carbon never realized utilization >50%. The enablement through the use of a metal oxide was partially due to a limited fluorine exchange with the oxide matrix as $Mo_3O_{11.2}F_{0.8}$ was identified in the best samples. All oxides resulted in a crystallographic transformation of the CuF_2 to distinctly different lattice parameters thought to be brought about by the fluorine abstraction or ion exchange with oxygen which may have assisted in the electrochemical activity of CuF_2. In addition, evidence of limited reversibility of the compound has been identified. The use of nanocomposites versus discrete nanomaterials overcame the volumetric packing considerations, typical to nanomaterials, and allowed good elevated temperature storage. Preliminary results have shown a possible volumetric energy density advantage over that of CF_x counterparts (Fig. 16).

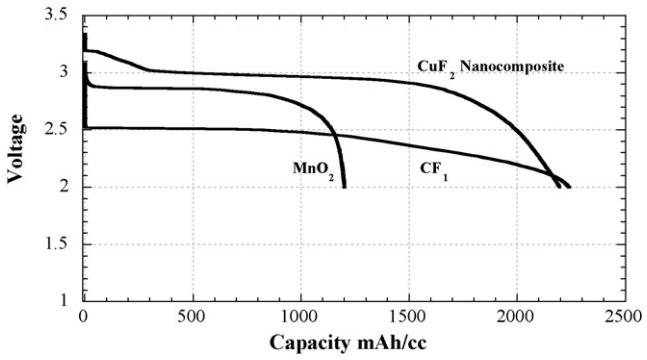

Fig. 16. Voltage profiles comparing the relative performance of MnO_2, HT(CF_1), and CuF_2 positive electrodes. Tests were performed vs. Li metal negative electrodes in 1 M $LiPF_6$ ethylene carbonate/dimethyl carbonate electrolyte at a rate of 7.58 mA/g at 24 °C. The calculated volumes are based on X-ray density (4.48 g/cm^3 MnO_2, 2.67 g/cm^3 CF_1, CuF_2 4.23 g/cm^3). All electrodes have discharged near theoretical capacities [123,124].

Although arguably not the most environmentally pleasing system, the Li/HgF_2 chemistry was investigated by Lerner and Seigler [125] for its relatively high theoretical OCV of 3.4 V. As with almost all the metal fluorides, HgF_2 is not conductive and is inhibited in performance. Although a relatively high OCV of 3.0 V was obtained, the voltage dropped to an average of 1.6 V under applied current. Although low voltage was induced by kinetic issues, the electrode achieved a high 80% utilization. Performance was seen to improve with the addition of Ag most likely through an amalgamation effect. The Li/CdF_2 chemistry was investigated in the same time period as an alternative to the poor performance and shelf life of Li–CuF_2 cells [126]. The purity of the cadmium fluoride precursor had a profound impact on the electrochemical activity, and progress was made in developing pure CdF_2 electrodes. Despite these advances, large overpotentials during discharge were identified which offset the observed 2.6 V OCV but good storage performance was identified relative to CuF_2 cells. In another report, a number of other metal fluoride systems have been investigated, most of them being based on their high open circuit voltage. Promising results of exceptional high voltage (5 V) metal fluorides were shown by Kronenberg [127]. A variety of very high voltage primary electrode materials such as CoF_3, NO_2SbF_6 and IF_5 were investigated. Some of these compounds such as CoF_3 exhibit a 5 V $1e^-$ discharge reaction. Although relatively unstable in the state of the art electrolytes, high performance and good shelf life were obtained when attention was made to electrolytes which would be stable at such extremely oxidizing potentials. Finally, BiF_3 was first investigated as a primary battery material in 1978 [128]. The cathode exhibited small utilization in the theoretical voltage region of 2.8–3.1 V, however a more extended region of reaction occurred below 2 V due to the formation of $Li_{3-x}Bi$ alloys. Although considerable amount of carbon additives were added to the electrode formulation, the electrochemical activity was restricted due to the insulating character of the BiF_3 compounds. There was discussion of the formation of a ternary compound Li_xBiF_3 during discharge, however no evidence of this was found in work performed 25 years later described in the next section.

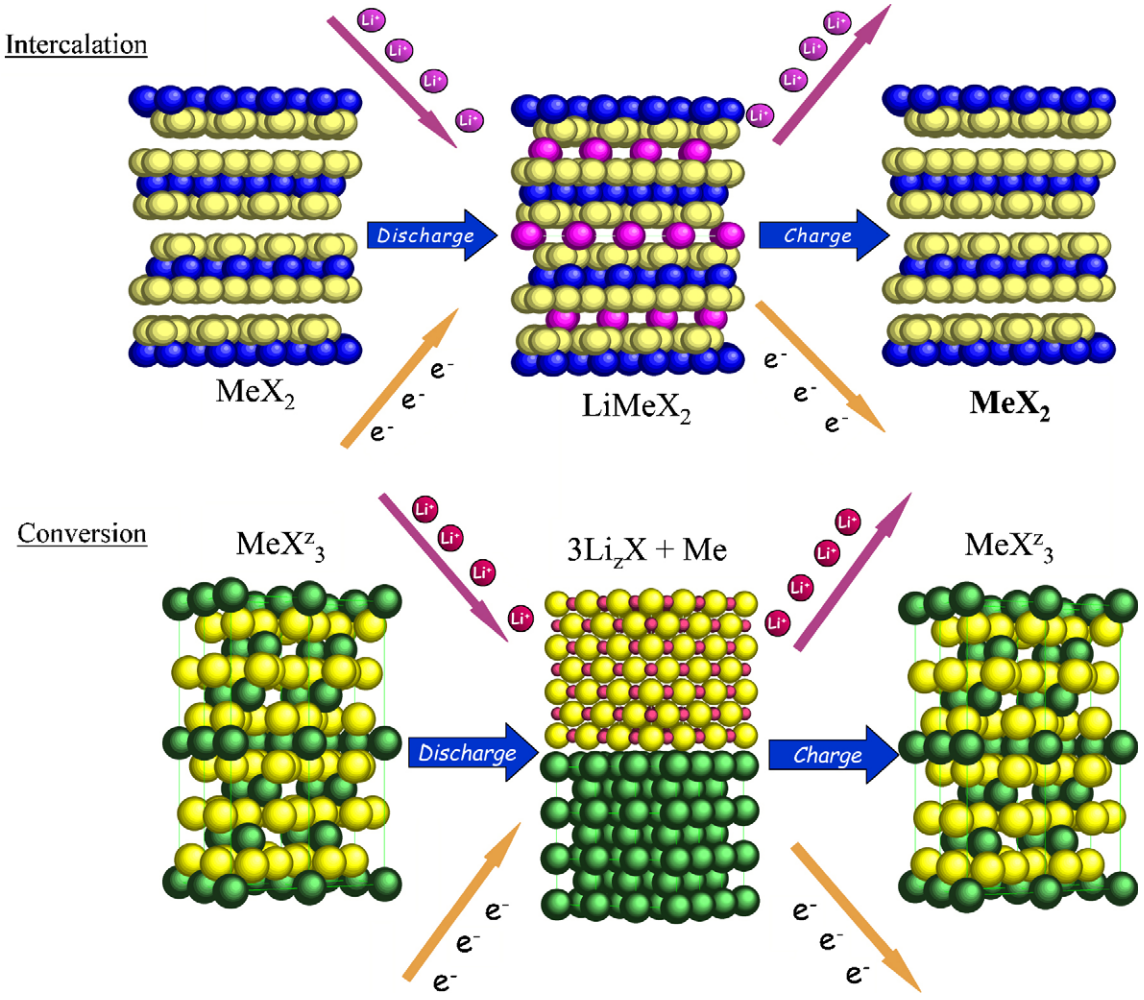

Fig. 17. Schematic showing contrasting crystallographic reaction mechanisms occurring during discharge of positive electrodes with reaction mechanisms based on intercalation and reversible conversion, respectively. Note the intercalation reaction demonstrates a total of 1 electron transfer (typically 250 mAh/g) whereas the conversion reaction can retain 3 electron transfer (typically >700 mAh/g).

4.2. Secondary nonaqueous batteries

All lithium secondary batteries utilize positive electrodes of intercalation compounds which retain their crystal structure upon lithium insertion. Although the lattice may expand, contract or distort slightly upon Li^+ insertion, the host structure remains intact (Fig. 17). Although the transition metals present in all of the intercalation compounds are capable of multiple electron transfer and thus higher capacity, the limited lithium vacancies inhibit the incorporation of more lithium and thus the charge transfer of more electrons to the structure. In addition, the covalency of the transition metal dichalcogenide bond reduces the voltage of the reaction. As seen above in the discussion of primary metal fluorides, the displacement/conversion process enables full utilization of all the redox potentials of the host metal as it reduces fully to the metallic state (4). Due to the fact that metal fluoride compounds are so highly ionic, this transition behaves quasi-ion like with redox potentials approaching that of free ions in solution. The metal fluoride conversion reaction leads to LiF and Me products which are on the scale of 2–5 nm. Due to the extremely small diffusion distances between these thermodynamically very stable reaction products, reversibility, and thus reformation of the MeF_x structure can occur on the following charge (Fig. 17) (5). The practical result is the theoretical improvement of the specific capacity of the positive electrode from 274 mAh/g for layered intercalation compounds to >700 mAh/g for the reversible conversion metal trifluorides.

$$xLi^+ + xe^- + MeF_x \leftrightarrow xLiF + Me \quad (5)$$

One of the first reports of a reversible metal fluoride for rechargeable lithium batteries was identified by Seiger et al. in 1970 [129]. Although voltage was lower than theoretical, the studies have shown that the first discharge of the NiF_2 could result in over 50% utilization and a limited degree of reversibility was shown in the electrochemical results with little self discharge during storage. The physical proof of the ability of fluorides to reversibly convert has been demonstrated by separate but parallel efforts of Hong et al. [130] and Badway et al. [131] three decades later. The former work was involved with the use of a TiF_3 compound. Reversible conversion was confirmed through the use of Raman spectroscopy which suggested the reformation of TiF_3. Electrochemical data showed multiple cycle reversibility (Fig. 18). The latter approach focused on higher voltage metal fluorides which are typically more insulating. In order to enable the electrochemical properties of such metal fluorides, FeF_3, FeF_2, NiF_2 and CoF_2, nanocomposites were fabricated with conductive carbon matrices. These nanocomposites were of relatively low surface area with nanocrystalline regions of MeF_x (10–30 nm) encapsulated by an amorphous carbon matrix (Fig. 19). Specific capacities in excess of 600 mAh/g and 400 mAh/g were demonstrated for FeF_3 and NiF_2, respectively. This approach has lead to the realization of the theoretical voltage of a wide variety of compounds including the aforementioned materials and CrF_3, CrF_2 and BiF_3. As discussed in the previous section, BiF_3 was investigated as a primary material in the past, but it never realized its full electrochemical performance as the material was studied in the macro state. The use of nanocomposites realized near theoretical specific capacity with theoretical volumetric energy densities approaching that of CF_x. The exceptional rate capability of these materials and reversibility has been shown to occur through the use of in situ XRD

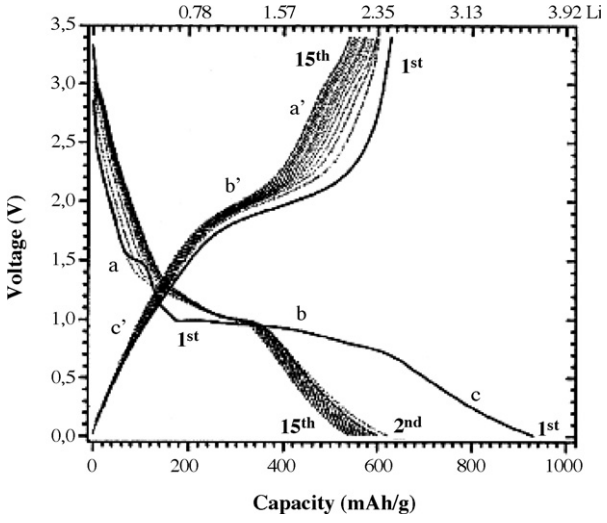

Fig. 18. Discharge and charge profiles of a TiF_3 electrode tested vs. a Li metal negative electrode using a $LiPF_6$ ethylene carbonate/dimethyl carbonate electrolyte. The cell was tested at 0.2 mA/cm^2 [130].

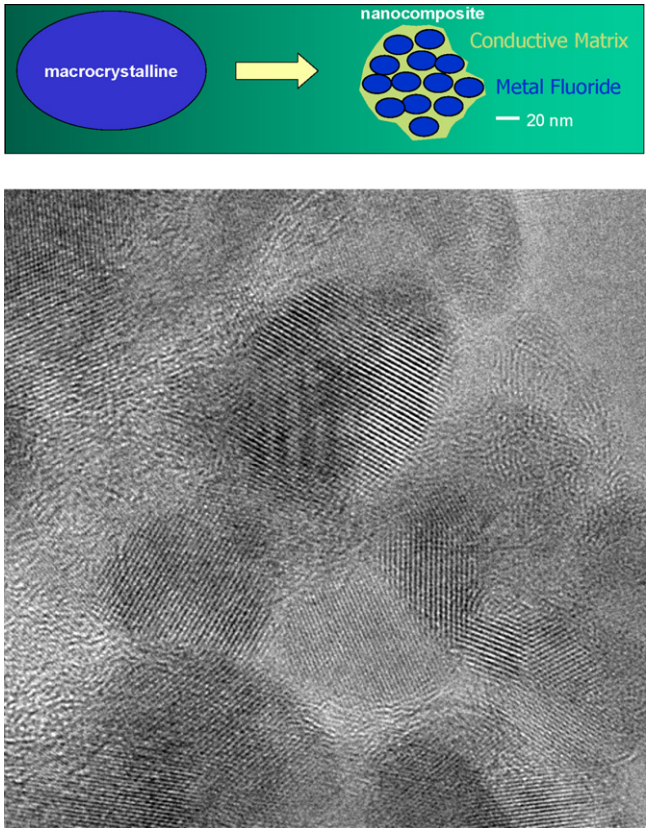

Fig. 19. HRTEM image of FeF_2 nanocomposite showing 10–20 nm nanocrystallites of FeF_2 in a matrix of amorphous carbon based on the idealistic metal fluoride nanocomposite schematic shown above.

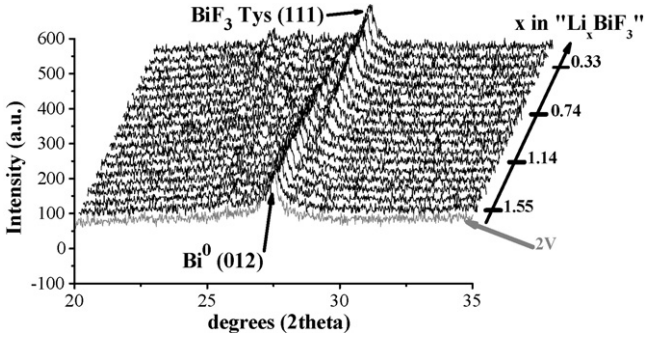

Fig. 20. In situ XRD patterns of the 3LiF:Bi discharge reaction product showing gradual reformation of the initial BiF_3 electrode during the anodic recharge (delithiation) reaction [132].

(Fig. 20) [132] and XAS. The reversible cycling of such materials were also shown by prefabricating 3LiF + Fe nanocomposites and cycling, thereby liberating lithium during the first charge to be utilized in a Li-ion configuration (Fig. 21) [133].

Many of the MeF_3 structures are related to the PdF_3-ReO_3 structures. Consisting of corner shared octahedrons and empty "A" sites, there is little to prevent shearing of the crystal structure leading to a large range of crystallographic distortions as one moves from the ReO_3 structure to the PdF_3 structure. These structures, which consist of corner shared MeF_6 octahedrons, form vacant octahedral interstices that allow the diffusion of lithium ions (Fig. 22). In light of the cation vacancies, many MeF_3 materials support intercalation, thereby forming Li_xMeF_3 compounds as was demonstrated by Arai et al. for TiF_3, FeF_3, and VF_3 [134]. It was later found that the MeF_x compounds supported a $1e^-$ intercalation region followed by the $2e^-$ conversion reaction resulting in the following (6) [135,136]:

$$Li^+ + e^- + MeF_3 \leftrightarrow LiMeF_3,$$
$$2Li^+ + 2e^- + LiMeF_3 \leftrightarrow 3LiF + Me \quad (6)$$

In the case of FeF_3 nanocomposites, the intercalation mechanism was found to be quite fast and very reversible. Even without the use of the higher capacity conversion reaction, the Li_xFeF_3 compound was shown to be an interesting 3 V intercalation material in its own right when formed as a nanocomposite.

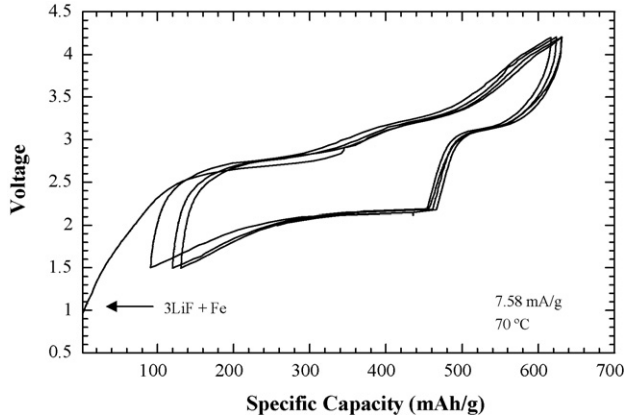

Fig. 21. The reversible cycling of a 3LiF/Fe/15%C nanocomposite in $LiPF_6$ ethylene carbonate/dimethyl carbonate electrolyte vs. a lithium negative electrode material at 7.58 mAh/g at 70 °C [133].

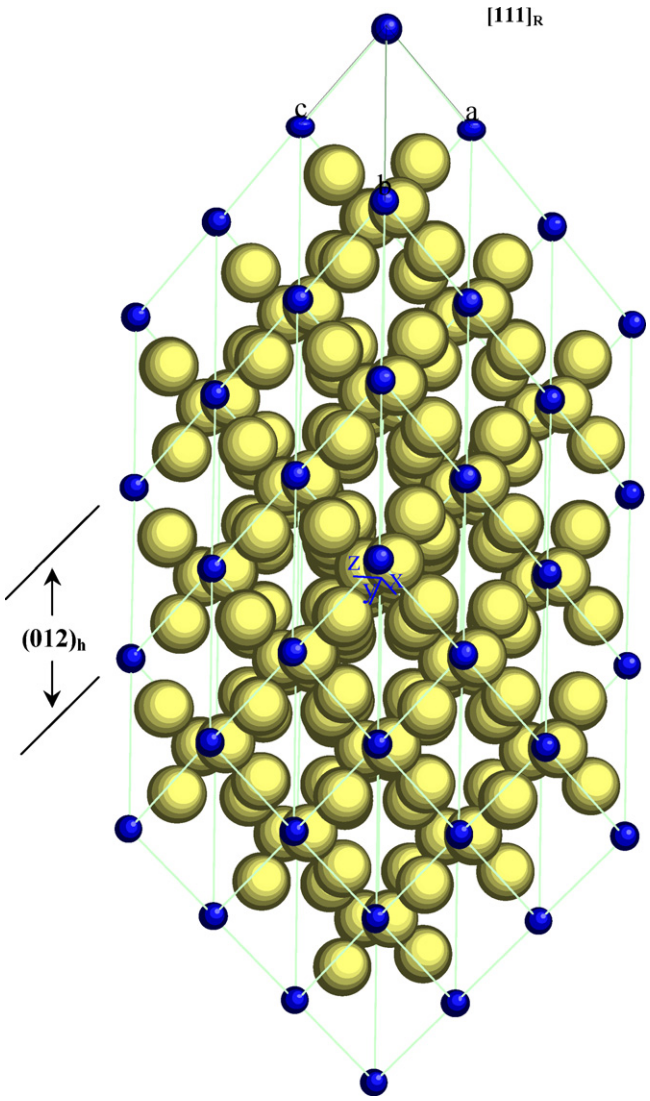

Fig. 22. Schematic showing the R-3C structure of FeF_3 [135].

Surpassing CuF_2 and BiF_3 in the important performance factor of volumetric energy density, much interest has been shown in AgF_2 as an ultrahigh energy density positive electrode material with a theoretical discharge voltage of 4.46 V. There have been reports of Li/AgF_2 cells in nonaqueous solutions of KPF_6 with discharge potentials of 3.4 V and 3.1 V corresponding to the discharge of AgF_2 and AgF [137]. Material utilization was on the order of 20–30% with little fade after 30–40 cycles. Peculiar was the use of Ag based positive electrode current collectors which had the propensity to place Ag^+ into solution during the anodic reaction on the positive electrode during charge. Therefore, it was difficult to identify what degree of the subsequent discharge was due to reconverted AgF_2 rather than to the effect of the reduction of Ag^+ ions in solution. However, this material may be of interest for further studies in applications where cost is not a major factor.

Synthesis of metal fluoride nanocomposite electrode materials have been reported through a novel mechanochemical

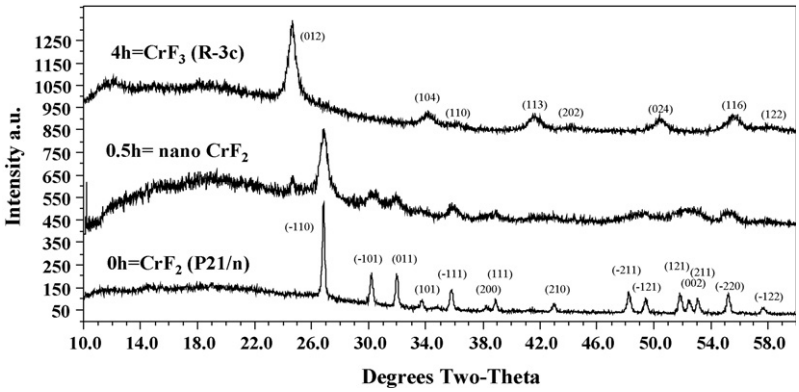

Fig. 23. XRD patterns showing formation of CrF_3 through the mechanochemically induced solid state reaction between CF and FeF_2 as a function of high energy milling time [138].

induced reaction [138]. Insulating CF_1 and MeF_2 compounds were reacted using high energy milling techniques resulting in a solid state redox reaction. This reaction was induced by the oxidation of the MeF_2 compound to MeF_3 by the oxidizing power of HT CF_1 (7). The resulting product was a fine nanocomposite of MeF_3 in a matrix of conducting carbon.

$$CF_1 + MeF_2 \rightarrow C + MeF_3 \quad (7)$$

The mechanochemical induced oxidation reaction was successfully carried out for $CrF_2 \rightarrow CrF_3$ (Fig. 23) and $FeF_2 \rightarrow FeF_3$. Such materials exhibited good reversibility and excellent capacities in excess of 600 mAh/g and 500 mAh/g, respectively. This technique worked for all metal fluorides with $Me^{2+} \rightarrow Me^{3+}$ redox levels below that of the theoretical oxidizing power of CF_1.

As with the previously discussed graphite oxide/fluoride chemistries, a similar question relating to the electrochemical activity of the oxyfluorides developed for the reversible conversion metal fluoride nanocomposites. This is of particular interest as reversible conversion has been shown to exist for oxides [139], nitrides [140], and sulfides. The question relating to oxyfluorides was addressed through a systematic array of bismuth oxyfluorides including $BiO_{0.5}F_2$ and BiOF [141] by Bervas et al. [142]. The electrochemical and subsequent physical characterization of the compounds during and after discharge revealed a sequential conversion of the oxyfluorides. The first step consisted in the conversion of the fluoride to LiF with the formation of a metastable bismuth oxide. The second plateau consisted of the conversion of the residual bismuth oxide to bismuth and Li_2O. During charge the compound first reconverted into bismuth oxide. Surprisingly, at higher voltages the compound did not reform BiF_3 but in fact reconverted to the original bismuth oxyfluoride (Fig. 24). The reported advantage of oxyfluorides is that small amounts of oxygen and its resulting covalency can induce drastic improvement in electronic conduction of the metal fluoride. The fact that oxygen can be reincorporated into the structure during reformation and recharge demonstrates that such an approach may be viable. In the case of bismuth with large amounts of oxygen, such incorporation was shown to lead to detrimental cycle life.

Although the reversible conversion metal fluorides are of great interest for their enormous energy densities which rival that of metal air and fuel cells when applied to smaller format batteries, there remains much to understand and improve relative to long term cycling stability and kinetics before such materials can be implemented into practical cells.

4.3. Thermal batteries

The high temperature (250–600 °C) environment of the thermal battery offers a unique opportunity to improve the

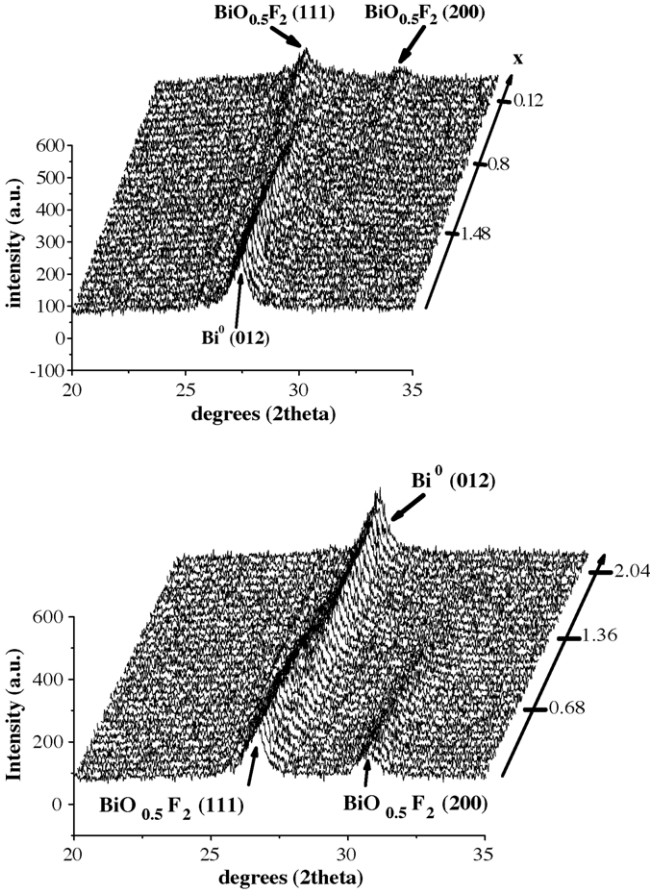

Fig. 24. In situ XRD patterns showing the conversion of $BiO_{0.5}F_2$ to Bi during the discharge (lithiation (lower)) reaction and the reformation of the phase upon recharge (delithiation (top)) [142].

kinetics and electronic transport of the poorly conductive metal fluoride electrode materials. One such thermal cell consists of molten salt electrolytes. In many cases, due to their low melting points, monovalent alkali chloride and bromide salts are utilized in thermal batteries. Due to the reactivity of the fluoride electrode materials such as CuF_2, AgF_2, and FeF_3, the use of fluoride electrolytes were necessitated [143]. High power primary thermal batteries utilizing fluoride electrodes of FeF_3, CrF_3, VF_4, MnF_3, K_2MnF_6, CuF_2, K_3CuF_6 and AgF_2 were investigated by Root and Sutala in a LiF–NaF–KF eutectic electrolyte at 500 °C versus a Mg anode [144]. Promising behavior was identified especially for the unique Cu^{3+} stabilized compound of K_3CuF_6. The high temperature environment of a thermal environment also enables the fast transport of other ions rather than Li^+. A radical deviation from this has been seen in the development of fluoride batteries where the active ion is the F^- anion rather than an alkali or alkaline earth cation. These cells are completely solid state and utilize a solid state F^- conductor as the electrolyte [145]. These cells use fast F^- conductors such as the extremely fast $Pb_xSn_yF_4$ phases with various anodes such as La and cathodes of high working potential based on Bi and Pb. Such cells are promising for operation in high temperature applications such as deep hole drilling.

4.4. Aqueous batteries

For a number of years, Ni/MH has been the mainstay of the high power, large size battery market. Such cells are found in hybrid electric vehicles and power tools and utilize KOH based aqueous electrolytes with a positive electrode composed of NiOOH and negative electrode of a hydrogen storing alloy AB_5, where A is a rare earth such as La and B is usually a first row transition metal such as Ni or Ti. In the development of higher capacity AB_2 Laves phase hydride alloys where A is Zr, Gao et al. investigated the fluorination effect on the $Zr_{0.9}Ti_{0.1}V_{0.2}Mn_{0.6}Ni_{1.3}La_{0.05}$ electrode [146]. Although AB_2 phase alloys normally result in higher energy density, they are typically hindered by poor initial activation, cycle life, and high rate capabilities. The fluorination procedure resulted in a factor of 20 larger surface area by the formation of a La based fluoride and the migration of Ni to the particle surface. These physical changes resulted in good performance compared with the AB_5 alloy due to a decrease in reaction resistance.

5. Summary

As energy storage cells such as the lithium battery enter a degree of maturity, the use of electrode materials containing fluorine is enabling new advances in both energy and stability. The introduction of oxyfluoride intercalation materials has brought forth improvements in the cycling, robustness, and storage of intercalation materials both at the positive and negative electrodes. Advances in characterization and synthesis are required to further identify the mechanistic basis for these results and control of the fluorine distribution, respectively. Carbon fluorides continue to offer outstanding specific energy, recent advances in low temperature processing through the use of oxidation aids or fullerene precursors offer the promise to a new age of improved performance and easier fabrication. After many years, a renaissance in the theoretically attractive, but electronically poor pure fluoride conversion materials has been initiated. The use of nanocomposite fluorides has offered a critical path to overcome the intrinsic barriers to ample electronic conductivity and ion transport and unleash the potential of these materials both as primary and secondary electrodes. Much work remains in the improvement of electrochemical energy storage quality factors such as cycle life, rate capability, and efficiency, but the promise of energy densities in excess of 100% of the current state of the art makes this a worthy effort. In short, the use of oxyfluoride and fluoride based cathodes in high energy density batteries has permeated a technology that already retains a wealth of fluorine chemistry in the form of electrolyte salts, solvents and binder materials.

Acknowledgements

The authors would like to thank A. Skrzypczak for his assistance in the preparation of this manuscript.

References

[1] D. Lemordant, F. Blanchard, G. Bosser, M. Caillon-Caravanier, B. Carre, A. Chagnes, B. Montigny, R. Naejus, in: T. Nakajima, H. Groult (Eds.), Fluorinated Materials for Energy Conversion, Elsevier, Amsterdam, USA, 2005, pp. 137–171.
[2] B.G. Nolan, S. Tsujioka, S.H. Strauss, in: T. Nakajima, H. Groult (Eds.), Fluorinated Materials for Energy Conversion, Elsevier, Amsterdam, USA, 2005, pp. 195–222.
[3] R. Jow, K. Xu, S. Zhang, M. Ding, US Patent 6 924 061 (2005).
[4] K.M. Abraham, J. Power Sources 14 (1985) 179–191.
[5] T. Nakajima, H. Groult (Eds.), Fluorinated Materials for Energy Conversion, Elsevier, Amsterdam, USA, 2005.
[6] C.W. Kwon, G. Campet, J. Portier, A. Poquet, L. Fournès, C. Labrugère, B. Jousseaume, T. Toupance, J.H. Choy, M.A. Subramanian, Int. J. Inorg. Mater. 3 (2001) 211–214.
[7] C.W. Kwon, H. Kim, T. Toupance, B. Jousseaume, C. Campet, in: T. Nakajima, H. Groult (Eds.), Fluorinated Materials for Energy Conversion, Elsevier, Amsterdam, USA, 2005, pp. 103–123.
[8] H.-W. Ha, K. Kim, M. de Borniol, T. Toupance, J. Solid State Chem. 179 (2006) 702–707.
[9] K. Kubo, M. Fujiwara, S. Yamada, S. Arai, M. Kanda, J. Power Sources 68 (1997) 553–557.
[10] C. Delmas, I. Saadoune, A. Rougier, J. Power Sources 43-44 (1993) 595–602.
[11] A. Rougier, I. Saadoune, P. Gravereau, P. Willman, C. Delmas, Solid State Ionics 90 (1996) 83–90.
[12] K. Kubo, S. Arai, S. Yamada, M. Kanda, J. Power Sources 81/82 (1999) 599–603.
[13] A.R. Naghash, J.Y. Lee, Electrochim. Acta 46 (2001) 2293–2304.
[14] A.R. Naghash, J.Y. Lee, Electrochim. Acta 46 (2001) 941–951.
[15] M. Guilmard, L. Croguennec, C. Delmas, J. Electrochem. Soc. 150 (2003) A1287–A1293.
[16] Y. Makimura, T. Ohzuku, J. Power Sources 119–121 (2003) 156–160.
[17] S.-H. Kang, I. Belharouak, Y.-K. Sun, K. Amine, J. Power Sources 146 (2005) 650–653.
[18] T. Ohzuku, Y. Makimura, Chem. Lett. 7 (2001) 642–643.
[19] N. Yabuuchi, T. Ohzuku, J. Power Sources 119–121 (2003) 171–174.
[20] G.-H. Kim, J.-H. Kim, S.-T. Myung, C.S. Yoon, Y.K. Sun, J. Electrochem. Soc. 152 (2005) A1707–A1713.

[21] G.-H. Kim, M.-H. Kim, S.-T. Myung, Y.K. Sun, J. Power Sources 146 (2005) 602–605.
[22] G.-H. Kim, S.-T. Myung, H.J. Bang, Jai Prakash, Y.K. Sun, Electrochem. Solid-State Lett. 7 (2004) A477–A480.
[23] H.-S. Shin, S.-H. Park, C.S. Yoon, Y.-K. Sun, Electrochem. Solid-State Lett. 8 (2005) A559–A563.
[24] M.-H. Lee, Y.-J. Kang, S.-T. Myung, Y.-K. Sun, Electrochim. Acta 50 (2004) 939–948.
[25] D.C. Li, T. Muta, L.Q. Zhang, M. Yoshio, H. Noguchi, J. Power Sources 132 (2004) 150–155.
[26] G. Amatucci, A. Du Pasquier, A. Blyr, T. Zheng, J.-M. Tarascon, Electrochim. Acta 45 (1999) 255–271.
[27] S. Jouanneau, J.R. Dahn, J. Electrochem. Soc. 151 (2004) A1749–A1754.
[28] S. Yonezawa, T. Okayama, H. Tsuda, M. Takashima, J. Fluorine Chem. 87 (1998) 141–143.
[29] M. Kageyama, D. Li, K. Kobayakawa, Y. Sato, Y.-S. Lee, J. Power Sources 157 (2006) 494–500.
[30] S.-H. Kang, K. Amine, J. Power Sources 146 (2005) 654–657.
[31] S.-H. Kang, Y.-K. Sun, K. Amine, J. Electrochem. Solid-State Lett. 6 (2003) A183–A186.
[32] G. Amatucci, J.M. Tarascon, U.S. Patent 5 674 645 (1997).
[33] G.G. Amatucci, A. Blyr, C. Schmutz, J.M. Tarascon, Prog. Batteries Battery Mater. 16 (1997) 1–19.
[34] J.T. Son, H.G. Kim, J. Power Sources 147 (2005) 220–226.
[35] G. Amatucci, U.S. Patent 5,759,720 (1998).
[36] G.G. Amatucci, N. Pereira, T. Zheng, I. Plitz, J.-M. Tarascon, J. Power Sources 81/82 (1999) 39–43.
[37] G. Amarucci, J.-M. Tarascon, J. Electrochem. Soc. 149 (2002) K31–K46.
[38] G. Amatucci, U.S. Patent 5 932 374 (1999).
[39] G.G. Amatucci, N. Pereira, T. Zheng, J.-M. Tarascon, J. Electrochem. Soc. 148 (2001) A171–A182.
[40] Y.-J. Kang, J.-H. Kim, Y.-K. Sun, J. Power Sources 146 (2005) 237–240.
[41] J. Xiao, H.-L. Zhu, Z.-Y. Chen, Z.-D. Peng, G.-R. Hu, Trans. Nonferrous Met. Soc. China 16 (2006) 467–472.
[42] S.-J. Bao, W.-J. Zhou, Y.-Y. Liang, B.-L. He, H.-L. Li, Mater. Chem. Phys. 95 (2006) 188–192.
[43] W. Choi, A. Manthiram, Electrochem. Solid-State Lett. 9 (2006) A245–A248.
[44] J.P. Remeika, J. Am. Chem. Soc. 76 (1954) 940–941.
[45] W. Xiaomei, Z. Xiangfu, Y. Qinghe, J. Zhongkao, W. Haoqing, J. Fluorine Chem. 107 (2001) 39–44.
[46] G.G. Amatucci, C.N. Shmutz, A. Blyr, C. Sigala, A.S. Gozdz, D. Larcher, J.-M. Tarascon, J. Power Sources 69 (1997) 11–25.
[47] B.-L. He, S.-J. Bao, Y.-Y. Liang, W.-J. Zhou, H. Li, H.-L. Li, J. Solid State Chem. 178 (2005) 897–901.
[48] P.S. Whitfield, I.J. Davidson, J. Electrochem. Soc. 147 (2000) 4476–4484.
[49] E. Wang, D. Ofer, W. Bowden, N. Iltchev, R. Moses, K. Brandt, J. Electrochem. Soc. 147 (2000) 4023–4028.
[50] S. Huang, Z. Wen, Z. Gu, X. Zhu, Electrochim. Acta 50 (2005) 4057–4062.
[51] T.-J. Kim, D. Son, J. Cho, B. Park, J. Power Sources 154 (2006) 268–272.
[52] S. Yonezawa, M. Takashima, in: T. Nakajima, H. Groult (Eds.), Fluorinated Materials for Energy Conversion, Elsevier, Amsterdam, USA, 2005, pp. 125–236.
[53] S. Yonezawa, M. Ohe, T. Tanida, M. Takashima, Abstr. 13th European Symp. on Fluorine Chemistry, vol. B25, 2001.
[54] T. Tanida, S. Yonezawa, M. Takashima, Abstr. 43rd Battery Symp., Japan, vol. 1A18, 2002.
[55] S. Yonezawa, M. Yamasaki, M. Takashima, J. Fluorine Chem. 124 (2004) 1657–1661.
[56] S. Yonezawa, M. Ozawa, M. Takashima, Tanso 205 (2002) 260–262.
[57] M. Takashima, S. Yonezawa, M. Ozawa, Mol. Cryst. Liq. Cryst. 388 (2002) 153–159.
[58] Y.-K. Sun, J.-M. Han, S.-T. Myung, S.-W. Lee, K. Amine, Electrochem. Commun. 8 (2006) 821–826.
[59] T. Nakajima, M. Koh, R.N. Singh, M. Shimada, Electrochim. Acta 44 (1999) 2879–2888.
[60] V. Gupta, T. Nakajima, Y. Ohzawa, H. Iwata, J. Fluorine Chem. 112 (2001) 233–240.
[61] T. Nakajima, V. Gupta, Y. Ohzawa, H. Iwata, A. Tressaud, E. Durand, J. Fluorine Chem. 114 (2002) 209–214.
[62] T. Nakajima, in: T. Nakajima, H. Groult (Eds.), Fluorinated Materials for Energy Conversion, Elsevier, Amsterdam, USA, 2005, pp. 31–59.
[63] H. Groult, T. Nakajima, L. Perrigaud, Y. Ohzawa, H. Yashiro, S. Komaba, N. Kumagai, J. Fluorine Chem. 126 (2005) 1111–1116.
[64] T. Nakajima, V. Gupta, Y. Ohzawa, M. Koh, R.N. Singh, A. Tressaud, E. Durand, J. Power Sources 104 (2002) 108–114.
[65] T. Zheng, W.R. McKinnon, J.R. Dahn, J. Electrochem. Soc. 143 (1996) 2137–2145.
[66] E. Peled, C. Menachem, D. Bar-Tow, A. Melman, J. Electrochem. Soc. 143 (1996) L4–L7.
[67] J.S. Xue, J.R. Dahn, J. Electrochem. Soc. 142 (1995) 3668–3677.
[68] T. Takamura, M. Kikuchi, Battery Tech. 7 (1995) 29–38.
[69] K. Matsumoto, Y. Ohzawa, T. Nakajima, B. Žemva, Z. Mazej, Abstr. 231st ACS National Meeting, Atlanta, USA, 2006.
[70] T. Nakajima, J. Li, K. Naga, K. Yoneshima, T. Nakai, Y. Ohzawa, J. Power Sources 133 (2004) 243–251.
[71] J. Li, K. Naga, Y. Ohzawa, T. Nakajima, A.I. Shames, A.M. Panich, J. Fluorine Chem. 126 (2005) 265–273.
[72] J. Li, K. Naga, Y. Ohzawa, T. Nakajima, H. Iwata, J. Fluorine Chem. 126 (2005) 1028–2035.
[73] K. Naga, Y. Ohzawa, T. Nakajima, Electrochim. Acta 51 (2006) 4003–4010.
[74] Y. Ohzawa, V. Gupta, B. Žemva, T. Nakajima, Abstr. 3rd French-Japanese Seminar on Fluorine in Inorganic Chemistry and Electrochemistry, Paris, France, (2003), pp. 25–27.
[75] H. Touhara, in: T. Nakajima, H. Groult (Eds.), Fluorinated Materials for Energy Conversion, Elsevier, Amsterdam, USA, 2005, pp. 61–88.
[76] J. Barker, M.Y. Saidi, J. Swoyer, U.S. Patent 6 387 568 (2002).
[77] J. Barker, M.Y. Saidi, J. Swoyer, J. Electrochem. Soc. 151 (2004) A1670–A1677.
[78] J. Barker, R.K.B. Gover, P. Burnes, A. Bryan, M.Y. Saidi, J. Swoyer, J. Electrochem. Soc. 152 (2005) A1776–A1779.
[79] J. Barker, R.K.B. Gover, P. Burnes, A. Bryan, M.Y. Saidi, J. Swoyer, J. Power Sources 146 (2005) 516–520.
[80] J. Barker, M.Y. Saidi, J. Swoyer, J. Electrochem. Soc. 150 (2003) A1394–A1398.
[81] J. Barker, R.K.B. Gover, P. Burnes, A. Bryan, Electrochem. Solid-State Lett. 8 (2005) A285–A287.
[82] J. Barker, M.Y. Saidi, J. Swoyer, Electrochem, Solid State Lett. 6 (2003) A1–A4.
[83] J. Barker, R.K.B. Gover, P. Burnes, A. Bryan, Electrochem. Solid-State Lett. 9 (2006) A190–A192.
[84] S. Okada, M. Ueno, Y. Uebou, J.I. Yamaki, J. Power Sources 146 (2005) 565–569.
[85] G. Ceder, Y.-S. Meng, Y. Shao-Horn, C.P. Grey, Meeting Abstract of IMLB-12, 2004, p. 24.
[86] Y. Koyama, I. Tanaka, H. Adachi, J. Electrochem. Soc. 147 (2000) 3633–3636.
[87] N. Wantanabe, Solid State Ionics 1 (1980) 87–110.
[88] N. Watanabe, R. Hagiwara, T. Nakajima, J. Electrochem. Soc. 131 (1984) 1980–1984.
[89] M. Fukuda, T. Iijima, in: J.-P. Gabano (Ed.), Lithium Batteries, Academic Press, London, 1983, pp. 211–238.
[90] N. Watanabe, M. Endo, K. Ueno, Solid State Ionics 1 (1980) 501–507.
[91] C. Julien, G. Nazri, Solid State Batteries: Materials Design and Optimization, Kluwer Academic Publishers, Boston, 1994, pp. 369–511.
[92] J. McBreen, H.S. Lee, X.Q. Yang, X. Sum, J. Power Sources 89 (2000) 163–167.
[93] R. Yazami, in: T. Nakajima (Ed.), Fluorine-Carbon and Fluoride-Carbon Materials, Marcel Dekker, Inc., New York, 1995, pp. 251–281.
[94] R. Hagiwara, T. Nakajima, N. Watanabe, J. Electrochem. Soc. 135 (1988) 2128–2133.

[95] M.S. Whittingham, J. Electrochem. Soc. 122 (1975) 526–527.
[96] W. Tiedemann, J. Electrochem. Soc. 121 (1974) 1308–1311.
[97] A. Hamwi, M. Daoud, J.C. Cousseins, Synth. Met. 26 (1988) 89–98.
[98] A. Hamwi, K. Guerin, M. Dubois, in: T. Nakajima, H. Groult (Eds.), Fluorinated Materials for Energy Conversion, Elsevier, Amsterdam, USA, 2005, pp. 369–395.
[99] T. Nakajima, M. Koh, V. Gupta, B. Žemva, K. Lutar, Electrochim. Acta 45 (2000) 1655–1661.
[100] V. Gupta, T. Nakajima, Y. Ohzawa, B. Žemva, Mol. Cryst. Liq. Cryst. 386 (2002) 25–31.
[101] T. Nakajima, V. Gupta, Y. Ohzawa, H. Groult, Z. Mazej, B. Žemva, J. Power Sources 137 (2004) 80–87.
[102] K. Guérin, R. Yazami, A. Hamwi, Electrochem. Solid-State Lett. 7 (2004) A159–A162.
[103] R. Yazami, A. Hamwi, Solid State Ionics 28 (1988) 1756–1761.
[104] A. Hamwi, M. Daoud, J.C. Cousseins, Synth. Met. 30 (1989) 23–31.
[105] Y. Matsuo, T. Nakajima, Electrochim. Acta 41 (1996) 15–19.
[106] A. Hamwi, C. Latouche, V. Marchand, J. Dupuis, R. Benoit, J. Phys. Chem. Solids 57 (1996) 991–998.
[107] D. Claves, J. Giraudet, A. Hamwi, J. Phys. Chem. B 105 (2001) 1739–1742.
[108] A. Hamwi, J. Phys. Chem. Solids 57 (1996) 677–688.
[109] J.H. Holloway, E.G. Hope, R. Taylor, G.J. Langley, A.G. Avent, T.J. Dennis, P.J. Hare, W.H. Kroto, R.M. Walton, J. Chem. Soc., Chem. Commun. 14 (1991) 966–969.
[110] N. Liu, H. Touhara, F. Okino, S. Kawasaki, Y. Nakacho, J. Electrochem. Soc. 143 (1996) 2267–2272.
[111] R. Yazami, Ph. Touzain, L. Bonnetain, Synth. Met. 7 (1983) 169–176.
[112] R.J. Lagow, R.B. Badachhape, J.L. Wood, J.L. Margrave, J. Chem. Soc., Dalton Trans. 96 (1974) 2628–2629.
[113] T. Nakajima, A. Mabuchi, R. Hagiwara, Carbon 26 (1988) 357–361.
[114] A.K. Tsvetnikov, T.Yu. Nazarenko, L.A. Matveenko, Yu.M. Nikolenko, Mater. Sci. Forum 91–93 (1992) 201–207.
[115] A. Hamwi, I. Al Saleh, D. Djurado, J.C. Cousseins, Mater. Sci. Forum 91–93 (1992) 245–249.
[116] A. Buteaux, A. Hamwi, D. Avignant, J. Dupuis, Mol. Cryst. Liq. Cryst. 310 (1998) 137–142.
[117] A. Hamwi, D. Claves, J. Fluorine Chem. 107 (2001) 241–245.
[118] J. Giraudet, D. Claves, A. Hamwi, Synth. Met. 118 (2001) 57–63.
[119] H.F. Bauman, in: Proceedings of the 20th Annual Power Sources Conference, May, PSC Publications, 1966, pp. 73–76.
[120] W.E. Elliott, J.R. Huff, G.L. Simmons, G.D. McDonald, J.L. Jamrozy, W.L. Towle, A Program to Develop a High-Energy Density Primary Battery With a Minimum of 200 Watt Hours Per Pound of Total Battery Weight, Contract report NASA CR-54873, December 31, 1965.
[121] S.G. Abens, T.X. Mahy, W.C. Merz, Development of High Energy Density Primary Batteries, Contract Report NASA CR-54859, December 28, 1965.
[122] J. Farrar, R. Keller, C.J. Mazac, in: Proceedings of the 18th Annual Power Sources Conference, May, PSC Publications, 1964, pp. 92–94.
[123] F. Badway, A.N. Mansour, J. Al-Sharab, N. Pereira, W.S. Yoon, F. Cosandey, I. Plitz, G.G. Amatucci, in: Proceedings of the 208th Meeting of the Electrochemical Society, October, Los Angeles, California, 2005.
[124] F. Badway, A.N. Mansour, J. Al-Sharab, N. Pereira, W.S. Yoon, F. Cosandey, I. Plitz, G.G. Amatucci, J. Electrochem. Soc., submitted for publication.
[125] S. Lerner, H.N. Seigler, J. Electrochem. Soc. 117 (1970) 574–575.
[126] M. Shaw, R. Chand, in: Proceedings of the 23rd Annual Power Sources Conference, May, PSC Publications, 1969, pp. 76–79.
[127] M.L. Kronenberg, in: Proceedings of the 36th Power Sources Conference, 1994, pp. 366–369.
[128] P. Fiordiponti, S. Panero, G. Pistoia, C. Temperoni, J. Electrochem. Soc. 125 (1978) 511–515.
[129] H.N. Seiger, A.E. Lyall, R.C. Shair, in: Proceedings of the 6th International Symposium on Power Sources 2: Res. Develop. Non-Mech. Elec. Power Sources, 1970, pp. 267–287.
[130] H. Li, G. Richter, J. Maier, Adv. Mater. 15 (2003) 736–739.
[131] F. Badway, F. Cosandey, N. Pereira, G.G. Amatucci, J. Electrochem. Soc. 150 (2003) A1318–A1327.
[132] M. Bervas, A.N. Mansour, W.-S. Woon, J.F. Al-Sharab, F. Badway, F. Cosandey, L.C. Klein, G.G. Amatucci, J. Electrochem. Soc. 153 (2006) A799–A808.
[133] F. Badway, N. Pereira, F. Cosandey, G.G. Amatucci, Mater. Res. Soc. Symp. Proc. 756 (2003).
[134] H. Arai, S. Okada, Y. Sakurai, J. Yamaki, J. Power Sources 68 (1997) 716–719.
[135] F. Badway, N. Pereira, F. Cosandey, G.G. Amatucci, J. Electrochem. Soc. 150 (2003) A1209–A1218.
[136] H. Li, P. Balaya, J. Maier, J. Electrochem. Soc. 151 (2004) A1878–A1885.
[137] M. Shaw, in: Proceedings of the 20th Annual Power Sources Conference, May, PSC Publications, 1966, pp. 70–73.
[138] I. Plitz, F. Badway, J. Al-Sharab, A. DuPasquier, F. Cosandey, G.G. Amatucci, J. Electrochem. Soc. 152 (2005) A307–A315.
[139] P. Poizot, S. Laruelle, S. Grugeon, L. Dupont, J.M. Tarascon, Nature (London) 407 (2000) 496–499.
[140] N. Pereira, L.C. Klein, G.G. Amatucci, J. Electrochem. Soc. 149 (2002) A262–A271.
[141] M. Bervas, B. Yakshinskiy, L.C. Klein, G.G. Amatucci, J. Am. Ceram. Soc. 89 (2006) 645–651.
[142] M. Bervas, L.C. Klein, G.G. Amatucci, J. Electrochem. Soc. 153 (2006) A159–A170.
[143] D.J. Briscoe, in: Proceedings of the 33rd Intersociety Energy Conversion Engineering Conference, 1998, pp. 1–5.
[144] A. Root, R. Sutala, in: Proceedings of the 22nd Annual Power Sources Conference, May, PSC Publications, 1968, pp. 100–102.
[145] G.W. Mellors, U.S. Patent 4 216 279 (1980).
[146] B. Liu, Z. Li, E. Higuchi, S. Suda, J. Alloys Compd. 293–295 (1999) 702–706.